NATIONAL ADVISORY COMMITTEE FOR AERONAUTICS

TECHNICAL NOTE 3959

CASCADE INVESTIGATION OF A RELATED SERIES OF 6-PERCENT-THICK GUIDE-VANE PROFILES AND DESIGN CHARTS

By James C. Dunavant

Langley Aeronautical Laboratory
Langley Field, Va.

Washington

May 1957

NATIONAL ADVISORY COMMITTEE FOR AERONAUT

TECHNICAL NOTE 3959

CASCADE INVESTIGATION OF A RELATED SERIES OF 6-PERCENT-THICK GUIDE-VANE PROFILES AND DESIGN CHARTS[1]

By James C. Dunavant

SUMMARY

A new blade series designed to operate at near choking inlet Mach numbers and to have near maximum critical Mach numbers by employing high aerodynamic loading of the profiles in the leading-edge region and relatively straight trailing edges is described. Low-speed cascade tests of four blade sections at solidities of 0.75, 1.00, and 1.50 were made over a wide range of angle of attack. From these tests, design angles of attack were selected and were used in a method of determining the camber for guide-vane turning angles as high as 50°. All turning angles measured at low drag conditions are plotted by the carpet-plotting method and from interpolation the necessary camber is readily obtainable for conditions other than those tested. A number of simple computations were made to estimate the high-speed characteristics of the blade series.

INTRODUCTION

Compressor designers have increased the weight flow and hence the axial Mach number entering the compressor as much as possible in attempting to obtain the maximum possible thrust per unit frontal area. The axial Mach number is too often limited by choking in the guide vanes. This choking has been avoided in some cases by eliminating the guide vanes and by designing the first rotor for axial entering flow. However, there is still a need for guide vanes in compressors including high weight-flow designs inasmuch as rotor efficiency usually decreases with increasing rotor tip Mach number in the transonic range. Using guide vanes permits the rotor tip Mach number to be lowered for the same weight flow and rotational speed.

At axial inlet Mach numbers of 0.5 to 0.7, the guide vanes will be required to operate at supercritical speeds, and at the higher turning

---

[1]Supersedes recently declassified NACA Research Memorandum L54I02 by James C. Dunavant, 1954.

angles the exit velocities will be near sonic. Guide-vane design, therefore, must consider the presence of shocks on the blades and the possibility of choking of the flow in the guide-vane passages.

Guide vanes which turn the flow efficiently and correctly have been designed from two-dimensional cascade data by using corrections for the change in axial velocity across the blade row such as are found in references 1 to 3. In the past, guide-vane design has largely used either circular-arc mean lines with arbitrary thickness distributions or the airfoil data obtained by Zimney and Lappi (ref. 4). An example of the former design is reference 5, which presents a method of designing circular-arc sheetmetal guide vanes that for many applications is satisfactory. However, none of these methods is entirely suitable for design of blades to operate at speeds considered necessary for high-speed compressors. Moreover, although the low-turning-angle data of Zimney and Lappi are systematic, their higher turning-angle data are not systematic and cannot be interpolated to other cambers.

The purpose of this investigation is to develop a related series of profiles designed specifically for guide-vane application at high subsonic speeds. Design information is presented for a new series of 6-percent-thick blade sections from results of low-speed cascade tests of these sections over a range of turning angles up to 50°, solidities of 0.75, 1.00, and 1.50, and design lift coefficients from 0.6 to 2.4. The analysis of results includes extrapolation of the pressure-distribution data by the method of reference 6 to give an indication of the high-speed characteristics, including the critical and choking Mach numbers. Also presented are some new turning-angle data for the NACA 65-(12)10 guide vanes, for which data were originally presented by Zimney and Lappi. These new data were obtained with improved cascade testing techniques.

SYMBOLS

A	area
c	blade chord
C_d	section drag coefficient
C_{l_o}	camber, expressed as a design lift coefficient of isolated airfoil
C_w	wake momentum difference coefficient
M	Mach number

p	static pressure
P	total pressure
P_R	resultant pressure coefficient: difference between local upper and lower surface pressure coefficients
q	dynamic pressure
s	tangential spacing between blades
S	pressure coefficient, $\frac{P - p}{q_1}$
V	velocity
x	chordwise distance from blade leading edge
y	perpendicular distance from blade chord line
α	angle of attack, angle between inlet flow direction and blade chord
β	air angle between flow direction and perpendicular to blade row, deg (see fig. 1)
σ	solidity, chord to spacing ratio (c/s)
θ	flow turning angle, deg

Subscripts:

1	upstream of blade row
2	downstream of blade row
T	throat

BLADE SECTION DESIGN

For compressors with high weight flow, the axial velocities entering the guide vanes may exceed the critical speed of the blade profile, and in some cases the exit velocities may even be sonic. Entering Mach numbers that produce sonic exit velocities are illustrated in figure 2(a)

as a function of turning angle for nonviscous one-dimensional flow through cascades of infinitely thin blades. Figure 2(b) shows the entering Mach number for which the blade passage chokes with no turning as a function of blade thickness and solidity.

The basic requirement of a high-speed guide-vane profile is good aerodynamic performance over a range of solidities and turning angles for maximum speeds before choking. This requirement means that (1) premature choking of the flow in the guide-vane passages must be avoided, and (2) airfoil profiles must be shaped to avoid shock waves so as to minimize shock-boundary-layer interaction effects and thereby to avoid separation and keep wake losses low. Only with data obtained in tests of profiles which meet these requirements can the flow into the first stage of the compressor be properly matched.

In order to arrive at suitable guide-vane profiles, a mean line and thickness distribution system of reference 7 was followed. The change in stream velocity through the passage was the primary consideration in selecting a mean line and hence the chordwise loading. In guide-vane applications the entering velocity is lower than the exit velocity and, therefore, the leading-edge region can be more highly loaded than the trailing-edge region and thereby delay supersonic velocities on the blade upper surface. This type of loading accomplishes most of the turning in the forward part of the passage and permits the use of lightly loaded, nearly straight trailing edges. The lightly loaded trailing edges are desirable because they provide less sensitivity of turning angle to variations in boundary layer, Reynolds number, turbulence, or surface finish.

The mean line used in this related series of guide-vane profiles is a combination of the $a = 0$ and the $a = 1.0$ mean lines of reference 7. The $a = 0$ mean line concentrates the loading near the leading edge. In order to remove the reflex curvature near the trailing edge which is characteristic of the $a = 0$ mean line, the uniform loading of the $a = 1.0$ mean line was added in the proportion of 4 to 6. The resulting mean line is designated the A_4K_6 mean line. This designation follows a system developed specifically for compressor and turbine profiles. (See the appendix of ref. 8.) In this system, the mean lines from $a = 1.0$ to $a = 0$ are identified by letters of the alphabet for each increment of 0.1, and the subscript indicates the proportions of the individual lift coefficients. Thus, the A_4K_6 mean line is the $a = 1.0$ mean line (A) with a $C_{l_o} = 0.4$ combined with the $a = 0$ mean line (K) with $C_{l_o} = 0.6$. The ordinates for this combined mean line for $C_{l_o} = 1.0$ are given in table I.

If high critical and high choking speeds are to be attained, it is necessary to have not only a thin blade section, as is seen from figure 2(b), but also a thickness distribution with the maximum thickness located well forward to permit the highest possible Mach number before choking, since turning the flow from the axial inlet direction contracts the passage toward the rear. These requirements are satisfied by the NACA 63-006 airfoil thickness distribution (ref. 7), for which the maximum thickness is located at 35 percent chord. The ordinates of this basic section were modified to give a thicker trailing edge by fairing a straight line from the trailing-edge radius, equal to 0.1 the maximum thickness, tangent to the upper and lower surfaces. Ordinates for this profile are given in table II. The airfoil series evolved is designated the NACA 63-$(C_{l_o}A_4K_6)$06 guide-vane profile.

APPARATUS AND PROCEDURE

Apparatus

The test apparatus was the high-aspect-ratio cascade tunnel described in reference 9, modified by reducing the test section width from 20 inches to 10 inches. Five-inch-chord blades were used so that the blade aspect ratio was 2.0. Seven blades were used in the cascade except in the case of the lowest solidity tests for which only five blades could be fitted into the tunnel. The side walls in the entrance to the test section contained an upstream boundary-layer suction slot. Solid test section side walls were used in all blade tests since reference 9 has shown that wall boundary-layer buildup by cascades accelerating the flow is insufficient to require the use of porous walls.

Five-inch-chord models were constructed of four blade cambers, $C_{l_o} = 0.6$, $C_{l_o} = 1.2$, $C_{l_o} = 1.8$, and $C_{l_o} = 2.4$. Two of the seven blade sets were constructed of plastic and two of metal. The center blade of each cascade contained a row of 22 static-pressure orifices distributed over the upper and lower surfaces at midspan.

The 65-$(12A_{10})$10 blade section of reference 4 was retested at aspect ratios of 1.0 and 2.0 in cascades with side-wall boundary-layer removal slots. Data from these tests are compared with the data from reference 4 which were obtained from tests with no boundary-layer removal slots.

Tests

The upstream flow angle was measured approximately one chord length upstream of the cascade at the tunnel center by means of a removable probe. The downstream angle was determined by averaging eight angular measurements taken approximately one-half chord length downstream of the midspan of the blades. Two measurements were taken behind each of the four centermost passages. These measurements were in a region in which no total-pressure loss had occurred.

Blades of each camber were tested at three solidities, $\sigma = 0.75$, 1.00, and 1.50, and through a range of angles of attack in 4° increments. The limits of the angle-of-attack range were determined by drag rise (drag coefficient values greater than twice the minimum drag coefficient) occurring at very high and very low angles of attack.

Turning angles were measured for a typical guide-vane cascade at Reynolds numbers from 260,000 to 100,000 to determine whether critical Reynolds numbers existed. Variation of the turning angle with Reynolds number in the range tested was 0.7°; hence, the test results for practical purposes were assumed to be unaffected by Reynolds number.

Because of the large variation in pressure ratio across the various cascades and the changes in upstream area, the blower was not able to supply either the pressure or the volume required to maintain a constant entering velocity for all the tests. Hence, the tests were run at maximum output of the blower and the resultant Reynolds number based on the upstream velocity and the 5-inch chord varied among tests from a minimum of 208,000 to a maximum of 294,000.

Blade forces were obtained by the method of reference 10. Normal forces determined by two methods, momentum change and integrated pressure distribution, were used as a check on testing technique accuracy. A maximum variation of 5 percent was permitted for acceptable tests except for conditions of low lift where a difference in coefficients of 0.05 was permitted.

RESULTS AND DISCUSSION

Aerodynamic Characteristics

Pressure distributions.- Low-speed cascade pressure distributions and blade section characteristics are shown in figures 3 to 14. As would be expected from the mean-line design, the pressure distributions show highest velocities over the upper surface as well as highest loading

in the leading-edge region. Generally, the pressure coefficients (and therefore the velocity) along the upper surface decreases from the leading-edge region to the trailing edge. Variations in solidity and camber change these characteristics only in altering the overall loading. An exception to this trend occurred in the test of the NACA 63-($24A_4K_6$)06 section at a solidity of 1.5, (fig. 14), where the highest turning angles of the tests were measured. In this instance the exit pressure coefficient approached that of the peak surface velocity in the leading-edge region; hence the pressure coefficient and velocity along the upper surface were almost constant. (See fig. 14.)

For many pressure distributions the pressure recovery over the upper surface was accompanied by a small laminar bubble located between the 40- and 70-percent-chord stations. The bubble usually moved toward the leading edge as the angle of attack was increased. Flow over the leading edge was evidently laminar, separated at the bubble (indicated by the flattening of the pressure distribution), and reattached as a turbulent boundary layer (indicated by sharp pressure rise immediately following the flattened separated region). Typical examples of this flow condition can be seen in the pressure distributions of figures 6, 7, and 9.

Turning angles.- Essentially uniform variations of turning angle θ with angle of attack α can be seen in the blade-test figures 3 to 14. Slopes of the curves for θ against α are approximately 1.0 except for the test for $\sigma = 0.75$, $C_{l_0} = 0.6$ (fig. 3(f)) in which the slope was significantly less. The data show that the largest increases in θ (at equal values of α) for a given increase in C_{l_0} occur at the highest solidity. For the lowest solidity ($\sigma = 0.75$) θ is increased only about 1° in increasing C_{l_0} from 1.8 to 2.4 but increases by 5° at the highest solidity ($\sigma = 1.5$).

Some effect of aspect ratio is present inasmuch as the tests were made with solid walls and are not exactly two-dimensional tests. Figure 15 shows a comparison of turning angles obtained for the NACA 65-($12A_{10}$)-10 blade section at aspect ratios of 1.0 and 2.0. Lower turning angles are produced by the aspect-ratio-1.0 blades for several reasons. The velocities induced by the trailing vortices due to reduced lift in the boundary-layer region as well as flow of the wall boundary layer onto the suction surface have a greater effect in decreasing the turning angle at the aspect-ratio-1.0 condition. Also, increases in the axial velocity due to the boundary layer which are greater at aspect ratio 1.0 have the effect of decreasing the turning angle. A more detailed discussion of this effect appears in reference 9.

The turning-angle data of Zimmey and Lappi for the 65-($12A_{10}$)10 blade sections (ref. 4) are shown also in figure 15. The discrepancy

between results for reference 4 and for the present tests is attributed to improved cascade testing techniques used in the present tests, the most important of which was the addition of wall slots for boundary-layer removal upstream of the blades.

Separation and drag.- Qualitative observations for separation were made by probing the passage with a small tuft. During the tests no separation of the flow was observed except as stall occurred at high and low angles of attack. At the lowest angle of attack the flow separated at the very leading edge of the lower surface. However, the flow reattached near the 50-percent-chord station. The constant-pressure region typical of this stall can be seen just behind the leading edge on the lower surface in figures 9(a) and 12(a). At high angles of attack, separation, when occurring, started on the upper surface at about the quarter-chord point and the flow did not become reattached. No attempt was made to record these tests because of the unsteadiness of the flow and the difficulty of obtaining accurate turning-angle measurements when the blade wakes extended completely across the blade passage.

Low drag values were obtained over a range of angles of attack from 10° to 18°. In this range, a design angle of attack was selected, by a method which is in the next section; the drag coefficients at design angle of attack are shown in figure 16(a). For equal design turning angles, lowest drag coefficients occur at the highest solidity as shown in figure 16(a). However, when drag is totaled for a number of blades to indicate all profile losses as in figure 16(b), minimum losses would be obtained at the lowest solidity tested (0.75) except for high turning at which a solidity of 1.00 would produce lower profile losses. Although lowering the solidity may reduce total blade profile losses, increases in secondary flows and Mach number effects that may accompany a decrease in the number of guide vanes may affect adversely the performance of subsequent blade rows. Although profile losses themselves constitute only a fraction of the total losses of a blade row there are indications that the blade surface boundary layer affects the secondary flow losses and hence blade profile losses may contribute more to total loss of a blade row near the blade end regions than the measured profile losses would indicate. Setting a lower limit on guide-vane solidity is illusory as the limit would vary with the particular application. However, it appears that guide vanes may be designed with solidities of 0.75 and lower in some applications.

Design angle of attack.- A design angle of attack was selected for each test condition to make the data obtained more usable for the design of entrance guide vanes. Each angle selected from the various pressure distributions is the highest angle of attack attained before the pressure distribution formed a sharp peak at the leading edge and also before drag rise occurred. The design angle of attack is shown in figure 17 for various turning angles and solidities plotted for accurate interpolation by the carpet-plotting method described in reference 11. No

abscissa scale is given for figure 17; however, turning angle and solidity values are plotted so that along a line of constant turning angle the smallest horizontal division is an increment of solidity of 0.005. Similarly, along a line of constant solidity the smallest horizontal division is an increment of turning angle equal to 0.2°.

In figure 18, test results of angle of attack, turning angle, solidity, and camber variations are plotted by the method described in reference 11. The limits of the angle-of-attack ranges plotted were the angles of attack at which twice the minimum drag occurs. From this plot, camber is readily determined for intermediate values of solidity, turning angle, and angle of attack. Camber for design angles of attack at solidities other than 1.5, 1.0, and 0.75, is obtained by entering figure 18 with the design angle of attack determined from figure 17 and the turning angle.

In figure 18, lines of constant turning angle and constant angle of attack are plotted to a horizontal scale with camber as the vertical scale. Each solidity forms a θ,α carpet plotted so that points of equal turning angle and angle of attack on the three θ,α carpets are spaced to a horizontal solidity scale. Hence, in order to interpolate for camber when the turning angle, angle of attack, and solidity are given, the point of the given turning angle and angle of attack is determined on the θ,α carpet for the three solidities 0.75, 1.0, and 1.5. The curve through these three points represents the variation in camber for solidities from 0.75 to 1.5 for the given combination of turning angle and angle of attack. Location of the point representing the given intermediate solidity is found by measuring, from a point of known solidity, turning angle, and angle of attack, a horizontal distance equivalent to the increment of solidity. For this carpet plot the smallest horizontal subdivision is equal to an increment in solidity of 0.002. The ordinate of the point thus located on the faired line is the desired camber.

Prediction of High-Speed Performance

Choking Mach numbers.- Although no high-speed cascade tests were made of the blade sections, a number of simple computations were made to estimate some of the high-speed characteristics of the blade series. The values estimated were the critical and choking Mach numbers. All of these analyses are based on the assumption that the low-speed turning angle would be obtained at all speeds up to choking. Although this assumption is not precisely valid, the variation in turning angle is expected to be smaller for these 63-series blades than for the blades of circular-arc camber lines of reference 12, which showed a maximum increase of about 2° at choking.

Choking in the blade rows is determined by the minimum passage or throat area, given for this blade series in figure 19(a). For fair comparison of throat areas of the three solidities, throat areas (A_T/A_1) are plotted against the low-speed design turning angles. The maximum entering Mach number determined from the ratio or throat area to upstream area and isentropic flow relationships is given in figure 19(b). For low design turning angles where the maximum flow area is restricted by the maximum blade thickness, higher maximum entering Mach numbers can be obtained by using low solidities as indicated in figures 19(a) and (b). However, for turning angles of 25° or greater, the maximum entering Mach number which can be obtained is essentially the same regardless of solidity since the minimum area, then at the trailing edge, varies little although a finite trailing-edge thickness was used. Figure 19(b) shows that for the design turning angles the choking entering Mach number is near the maximum obtainable for the resulting low-speed turning angle.

Critical Mach numbers.- The entrance Mach numbers associated with the first occurrence of sonic velocity on the blade surface for the blade sections at design angle of attack were estimated by using low-speed cascade pressure distributions and correcting for the effects of compressibility as in reference 6. Figure 19(c) shows the critical Mach number for blade sections at design angle of attack. For low design turning angles differences in critical Mach number for the various solidities are small; however, for high design turning angles significant differences are shown. Although exceeding the critical speed cannot be taken as a positive indication of increased losses, speeds up to critical are expected to show no appreciable change in losses. The effect of high Mach numbers on the low-speed pressure distribution is to shift the loading toward the trailing edge. This effect is insignificant for low turning angles; however, for high turning angles the changes are pronounced. The low-speed and extrapolated pressure distributions of a typical high turning angle section ($\theta = 50.6°$) are shown in figure 20.

SUMMARY OF RESULTS

Guide-vane blade sections have been designed to provide such qualities believed desirable for guide vanes such as high aerodynamic loading in the leading-edge region, relatively straight trailing edges, and low maximum thickness. From low-speed cascade tests and analysis of performance at high speeds the blade sections are shown to have the following characteristics:

1. Low drag coefficients were obtained over an angle-of-attack range from 10° to 18°. No turbulent separation of the flow was detected near the selected design angle of attack.

2. The relatively straight trailing edges of the blade series were effective in guiding the flow at the trailing edges since the variation of turning angle with angle of attack was uniform.

3. High loading of the mean line in the leading-edge region produced high loading in this region for most cascade conditions; however, at the highest of turning angles, pressures along the upper surface were almost constant.

4. At the design angle-of-attack condition for turning angles greater than 25° the choking area corresponded to an entering Mach number which is near the maximum obtainable for the resulting low-speed turning angle. For lower turning angles the maximum entering Mach number is limited by the blockage because of maximum blade thickness.

Langley Aeronautical Laboratory,
Nation Advisory Committee for Aeronautics,
Langley Field, Va., August 19, 1954.

REFERENCES

1. Kahane, A.: Investigation of Axial-Flow Fan and Compressor Rotors Designed for Three-Dimensional Flow. NACA TN 1652, 1948.

2. Beatty, Loren A., Savage, Melvyn, and Emery, James C.: Experimental Investigation of Flow Through Three Highly Loaded Inlet Guide Vanes Having Different Spanwise Circulation Gradients. NACA RM L52D25a, 1952.

3. Lieblein, Seymour, and Ackley, Richard H.: Secondary Flows in Annular Cascades and Effects on Flow in Inlet Guide Vanes. NACA RM E51G27, 1951.

4. Zimney, Charles M., and Lappi, Viola M.: Data for the Design of Entrance Vanes From Two-Dimensional Tests of Airfoils in Cascade. NACA WR L-188, 1945. (Formerly NACA ACR L5G18.)

5. Lieblein, Seymour: Turning-Angle Design Rules for Constant-Thickness Circular-Arc Inlet Guide Vanes in Axial Annular Flow. NACA TN 2179, 1950.

6. Dunavant, James C., and Erwin, John R.: Investigation of a Related Series of Turbine-Blade Profiles in Cascade. NACA TN 3802, 1956 (Supersedes NACA RM L53G15.)

7. Abbott, Ira H., von Doenhoff, Albert E., and Stivers, Louis S., Jr.: Summary of Airfoil Data. NACA Rep. 824, 1945. (Supersedes NACA WR L-560.)

8. Erwin, John R., and Yacobi, Laura A.: Method of Estimating the Incompressible-Flow Pressure Distribution of Compressor Blade Sections at Design Angle of Attack. NACA RM L53F17, 1953.

9. Erwin, John R., and Emery, James C.: Effect of Tunnel Configuration and Testing Technique on Cascade Performance. NACA Rep. 1016, 1951. (Supersedes NACA TN 2028.)

10. Herrig, L. Joseph, Emery, James C., and Erwin, John R.: Systematic Two-Dimensional Cascade Tests of NACA 65-Series Compressor Blades at Low Speeds. NACA TN 3916, 1957. (Supersedes NACA RM L51G31.)

11. Felix, A. Richard: Summary of 65-Series Compressor-Blade Low-Speed Cascade Data by Use of the Carpet-Plotting Technique. NACA TN 3913, 1957. (Supersedes NACA RM L54H18a.)

12. Lieblein, Seymour, and Sandercock, Donald M.: Compressibility Correction for Turning Angles of Axial-Flow Inlet Guide Vanes. NACA TN 2215, 1950.

TABLE I.- COORDINATES FOR A_4K_6 MEAN LINE

$[c_{l_o} = 1.0]$

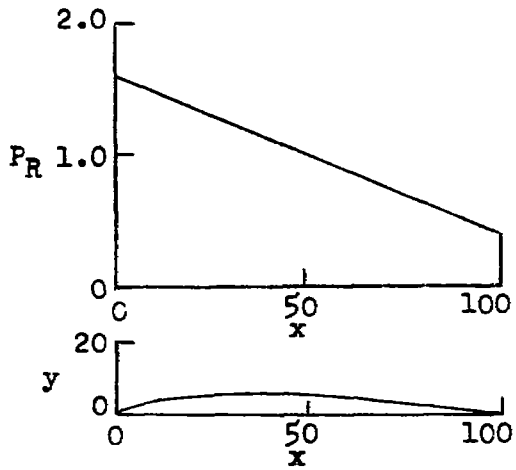

x	y	dy/dx
0	0	------
.5	.376	0.6237
1.25	.792	.5034
2.5	1.357	.4100
5.0	2.248	.3131
10	3.531	.2110
15	4.420	.1483
20	5.040	.1023
25	5.458	.0659
30	5.710	.0359
35	5.824	.0104
40	5.820	-.0116
45	5.713	-.0308
50	5.516	-.0478
55	5.239	-.0628
60	4.891	-.0761
65	4.479	-.0881
70	4.011	-.0990
75	3.492	-.1090
80	2.922	-.1184
85	2.308	-.1278
90	1.642	-.1387
95	.912	-.1555
100	0	------

TABLE II.- THICKNESS DISTRIBUTION COORDINATES FOR NACA 63-006 AIRFOIL WITH TRAILING EDGE THICKENED (t/c = 6 PERCENT)

[Stations and ordinates given in percent of chord]

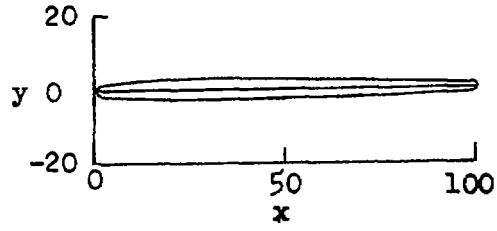

x	±y
0	0
1.25	.771
2.5	1.057
5.0	1.462
10	2.010
15	2.386
20	2.656
25	2.841
30	2.954
35	3.000
40	2.971
45	2.877
50	2.723
55	2.517
60	2.301
65	2.085
70	1.870
75	1.654
80	1.438
85	1.222
90	1.007
95	.791
100	0
L. E. radius:	0.297
T. E. radius:	0.6

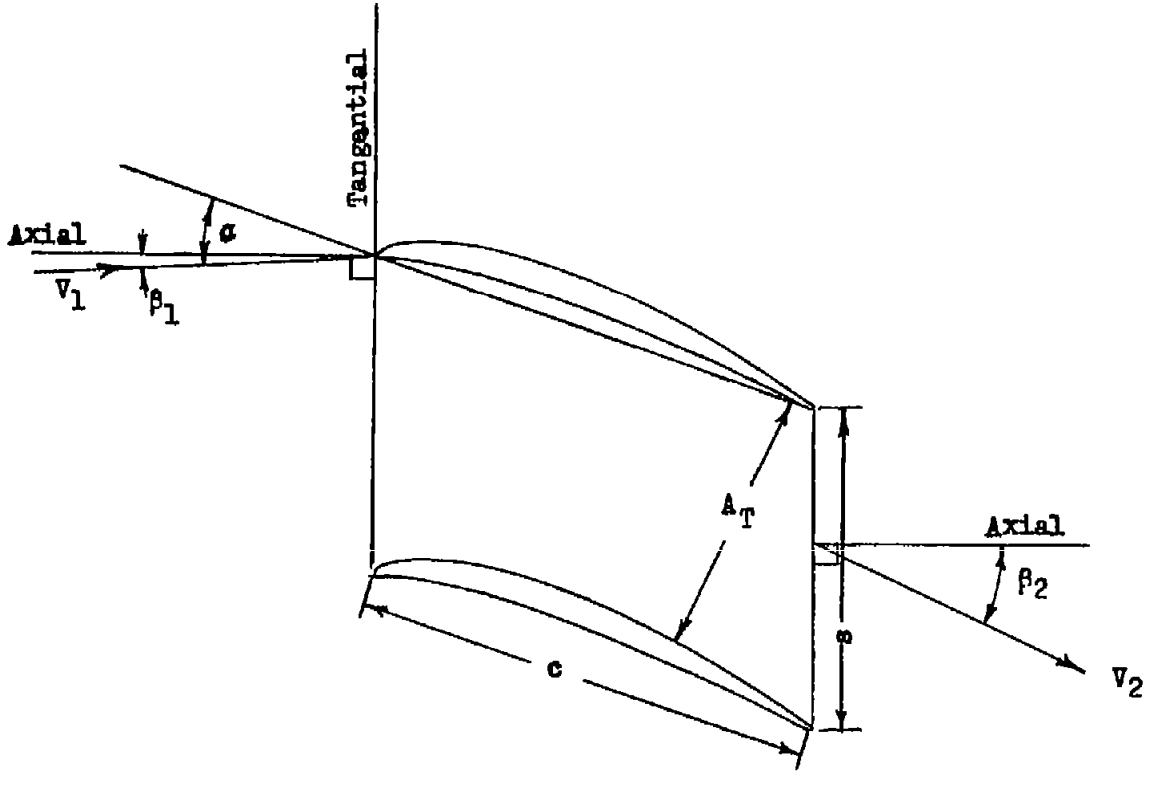

Figure 1.- Cascade notation.

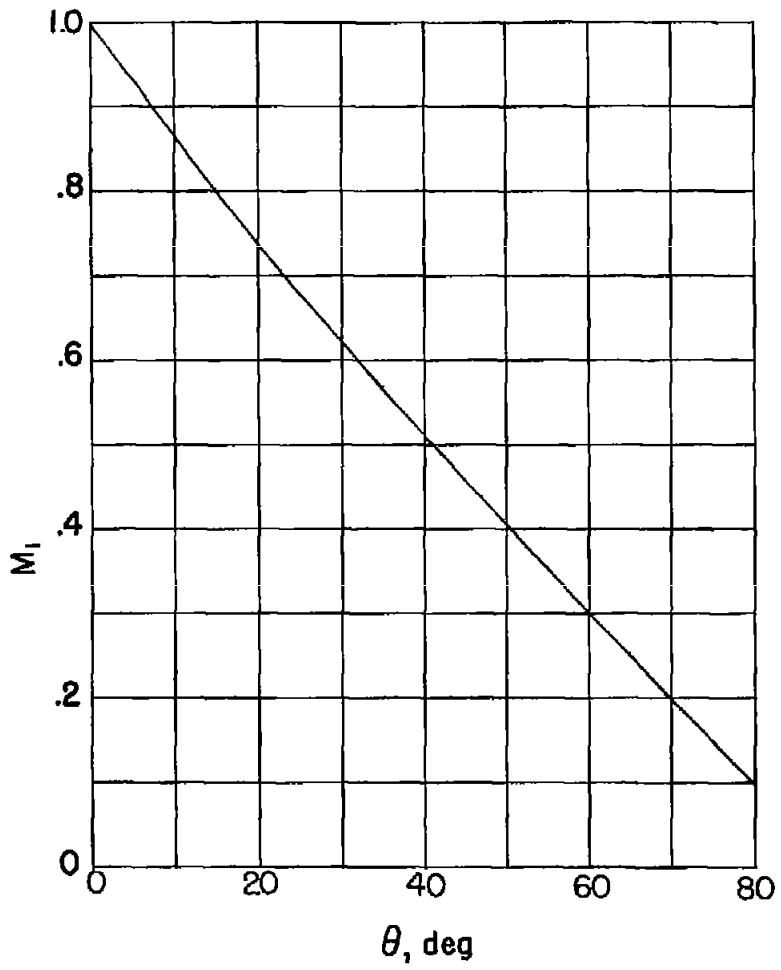

(a) Turning angle for sonic exiting velocity.

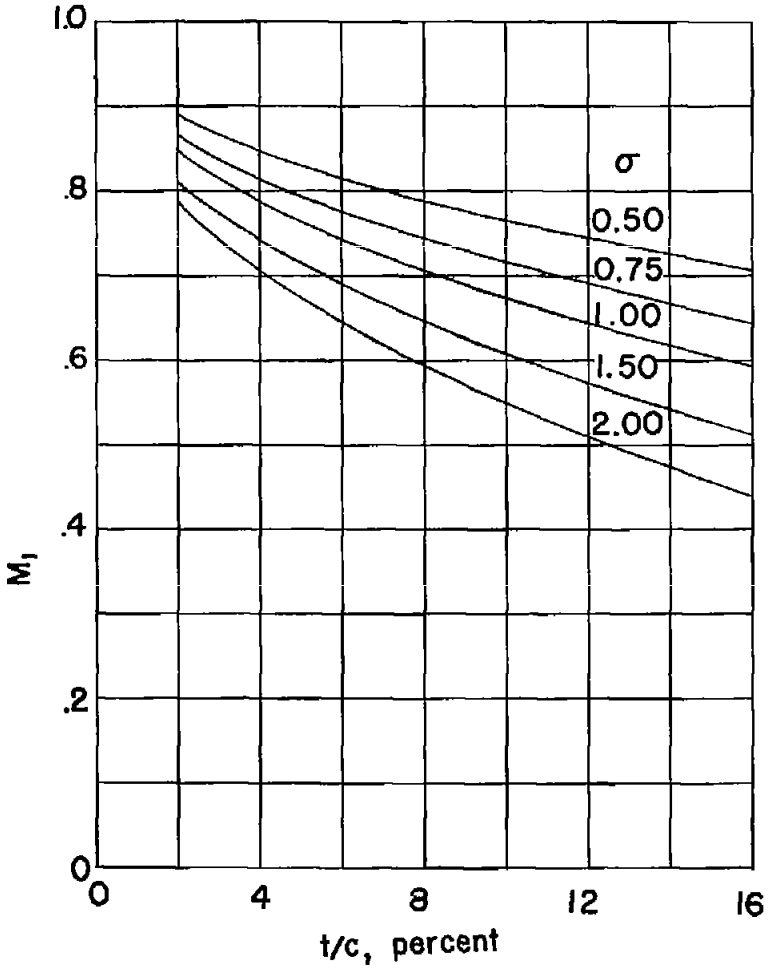

(b) Maximum blade thickness and solidity for choking in the blade passage. $\theta = 0^{\circ}$.

Figure 2.- Maximum entering Mach number for two-dimensional guide-vane cascades ($\beta_1 = 0^{\circ}$).

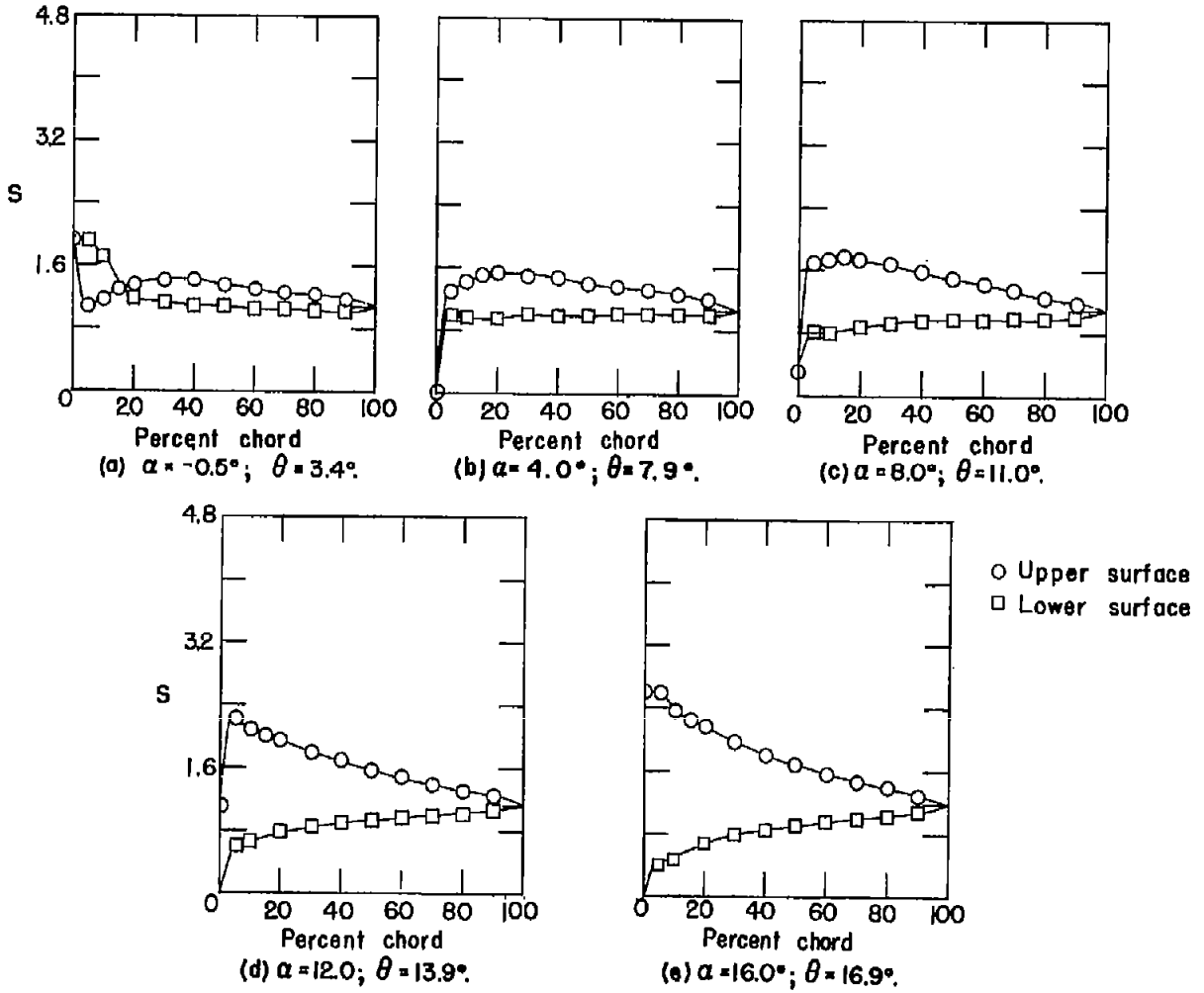

Figure 3.- Blade-surface pressure distributions and blade section characteristics for cascade combination, $\beta_1 = 0^\circ$, $\sigma = 0.75$, and NACA 63-($6A_4K_6$)06 blade section.

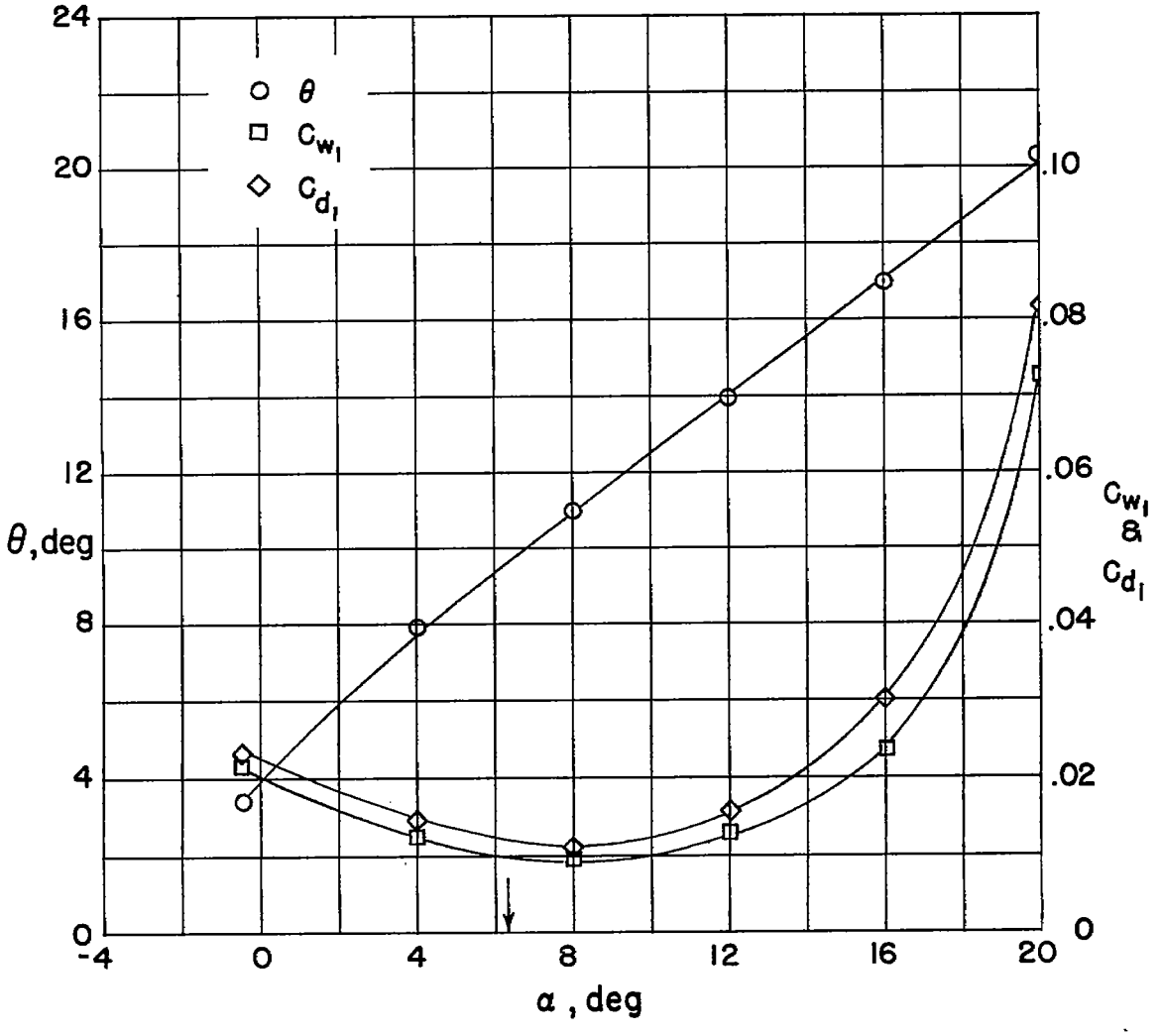

(f) Section characteristics. Arrow shows design angle of attack.

Figure 3.- Concluded.

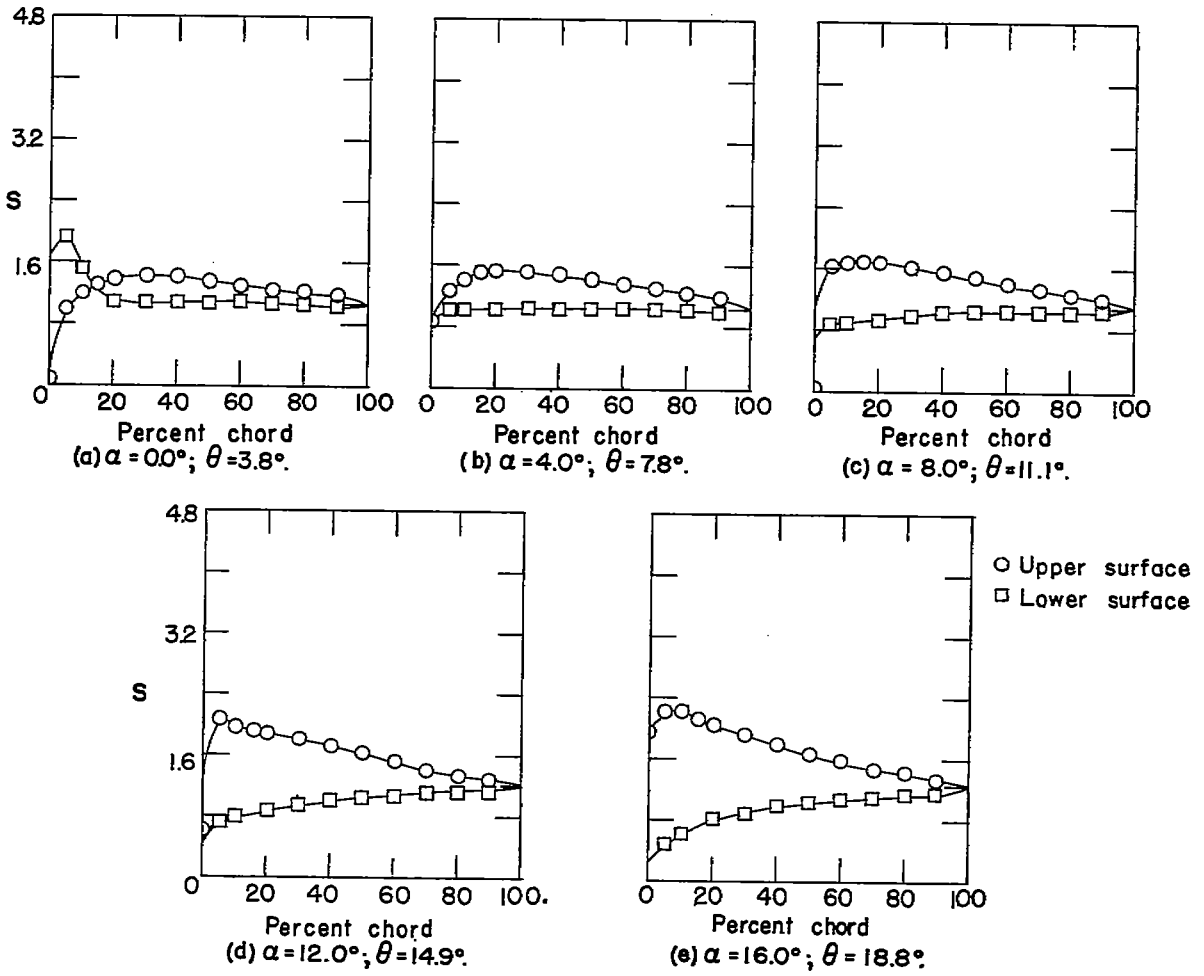

Figure 4.- Blade-surface pressure distributions and blade section characteristics for cascade combination, $\beta_1 = 0^\circ$, $\sigma = 1.0$, and NACA 63-($6A_4K_6$)06 blade section.

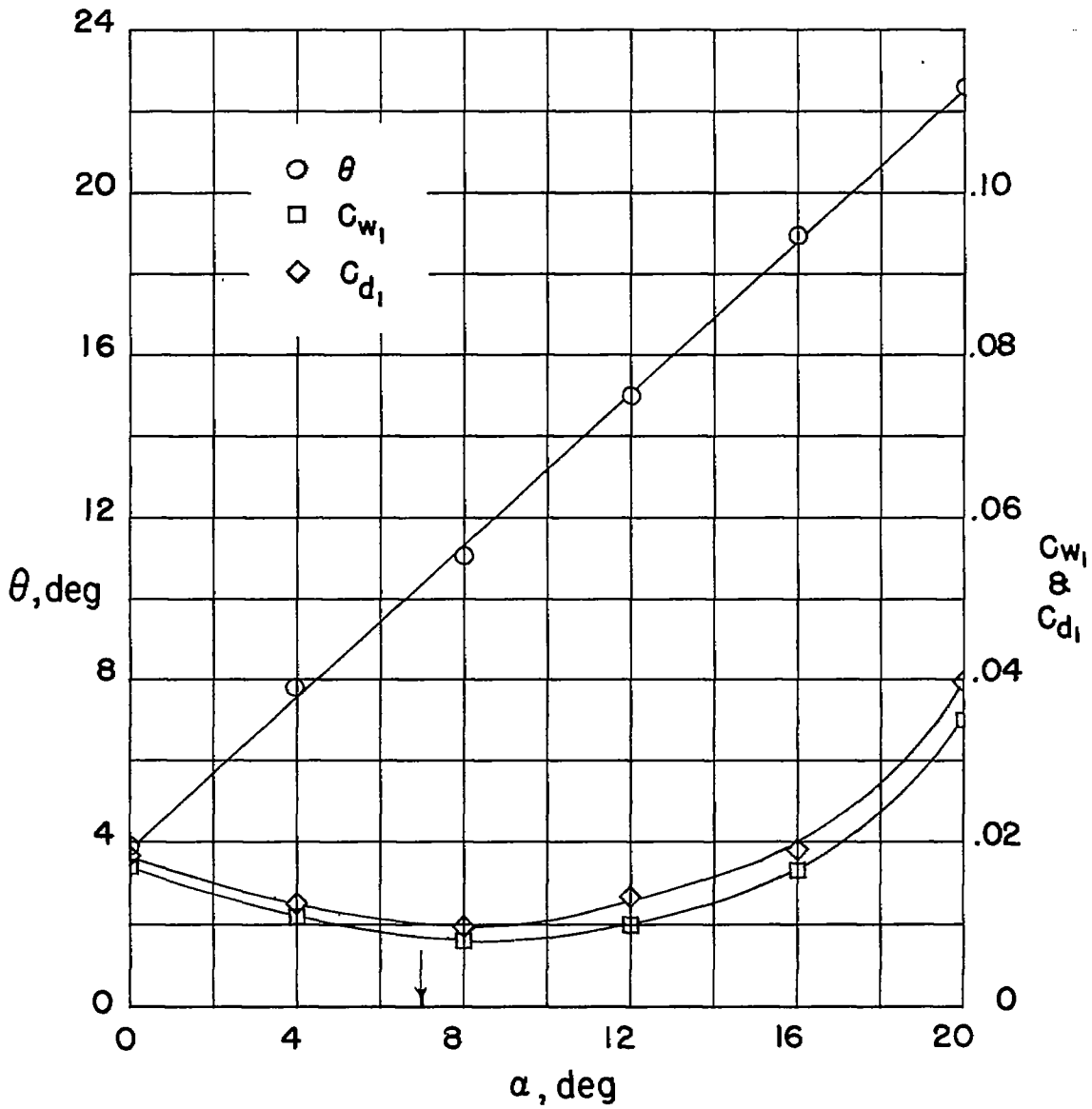

(f) Section characteristics. Arrow shows design angle of attack.

Figure 4.- Concluded.

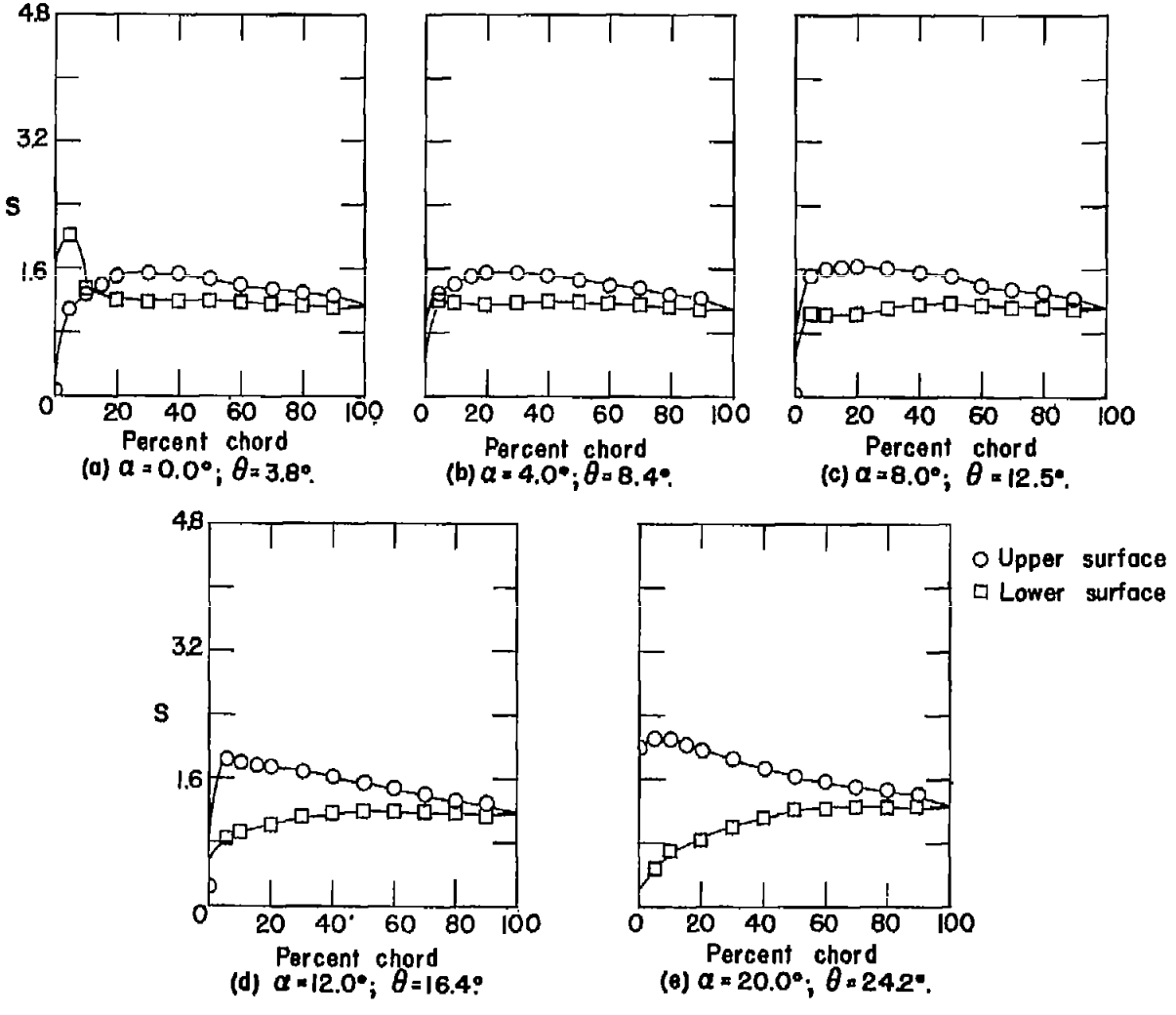

Figure 5.- Blade-surface pressure distributions and blade section characteristics for cascade combination, $\beta_1 = 0^\circ$, $\sigma = 1.5$, and NACA 63-($6A_4K_6$)06 blade section.

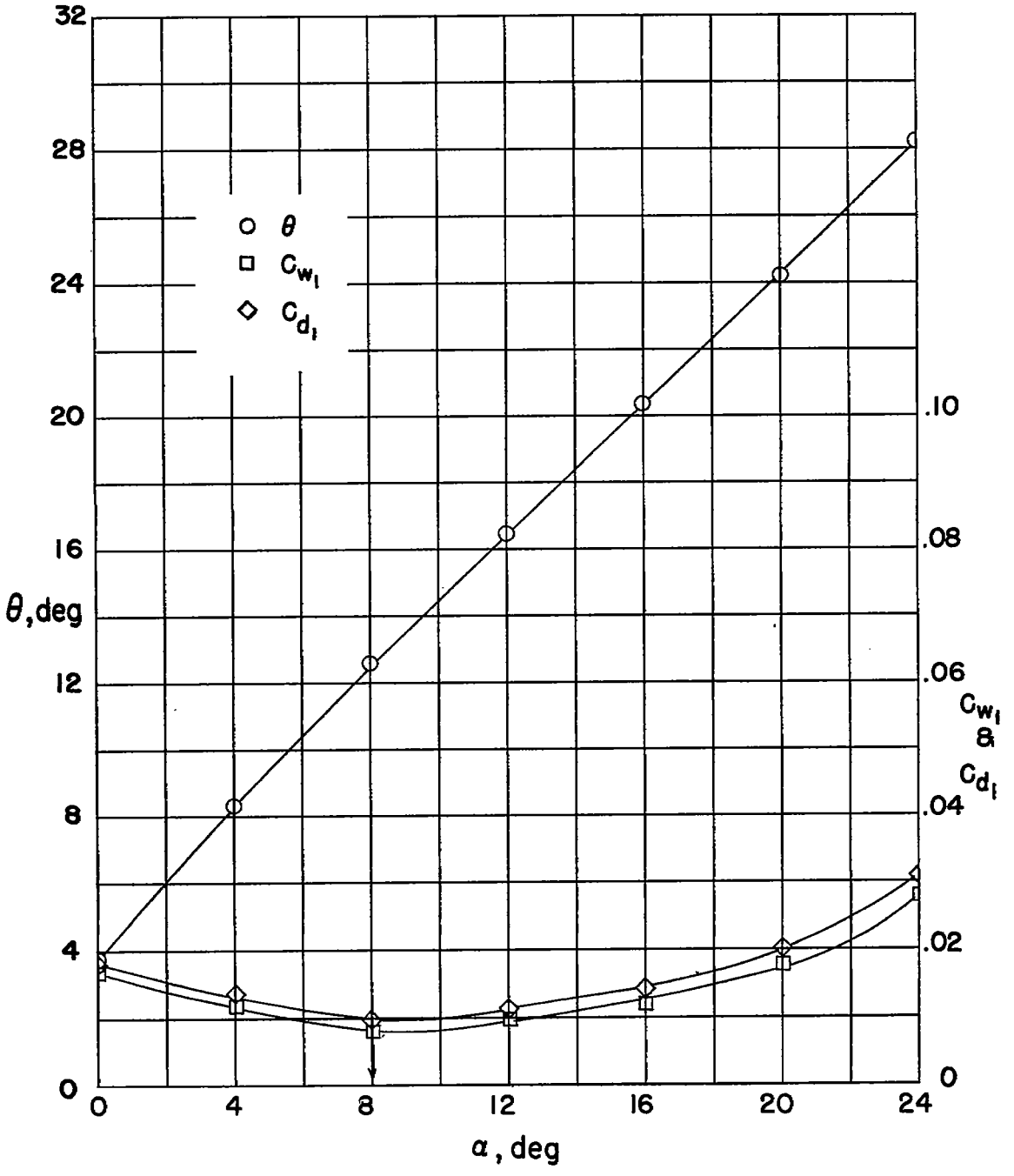

(f) Section characteristics. Arrow shows design angle of attack.

Figure 5.- Concluded.

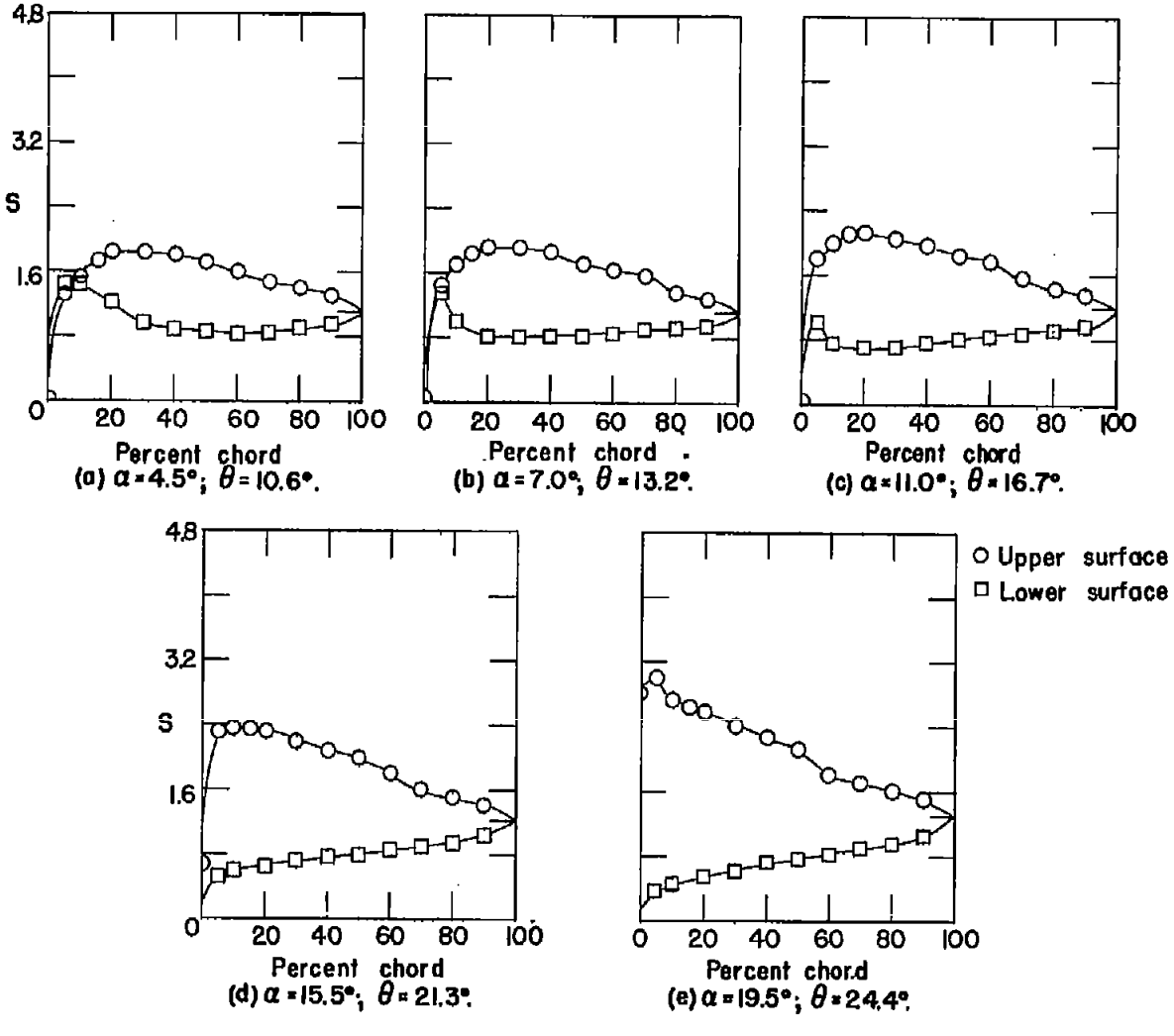

Figure 6.- Blade-surface pressure distributions and blade section characteristics for cascade combination, $\beta_1 = 0^\circ$, $\sigma = 0.75$, and NACA 63-($12A_4K_6$)06 blade section.

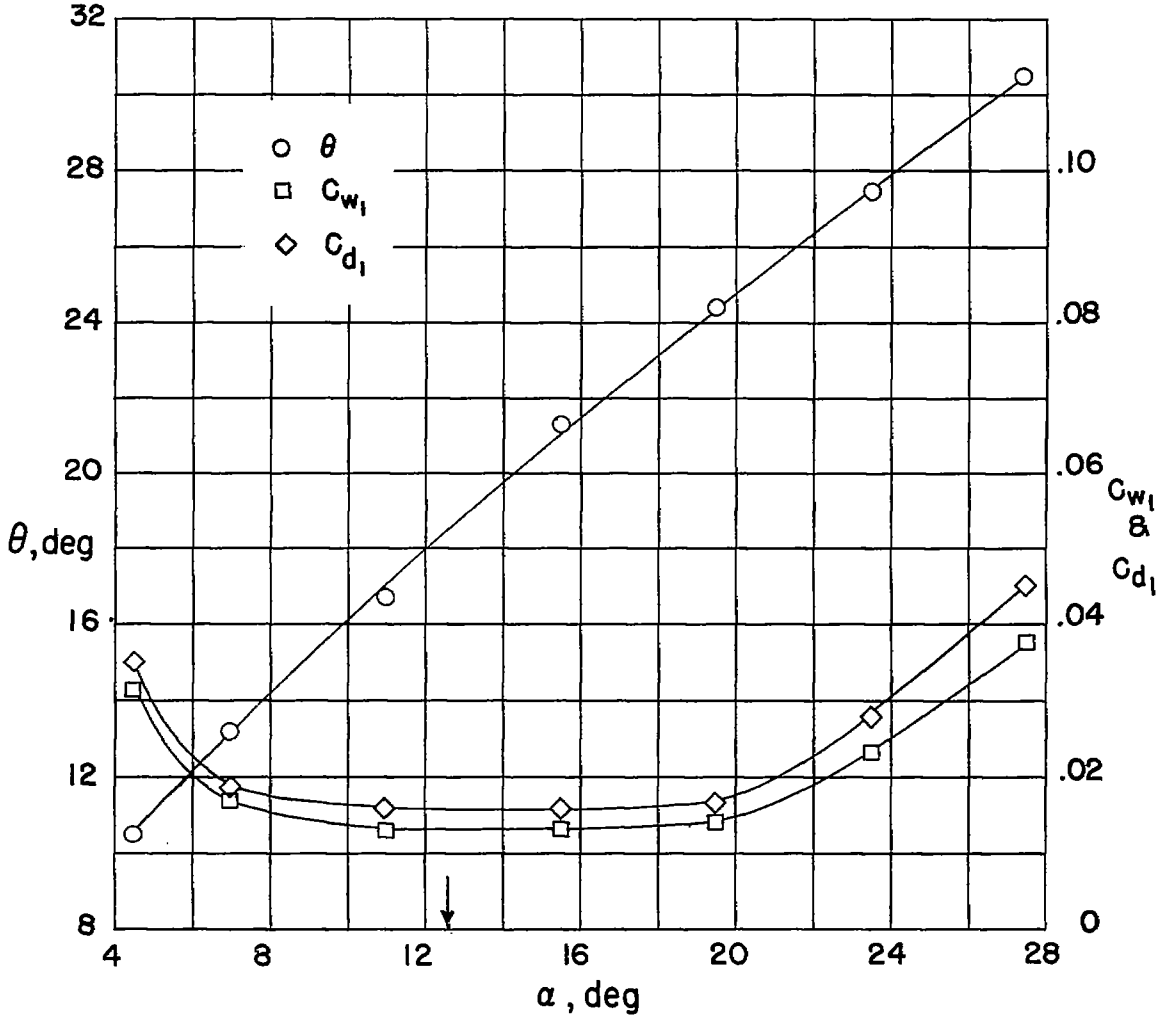

(f) Section characteristics. Arrow shows design angle of attack.

Figure 6.- Concluded.

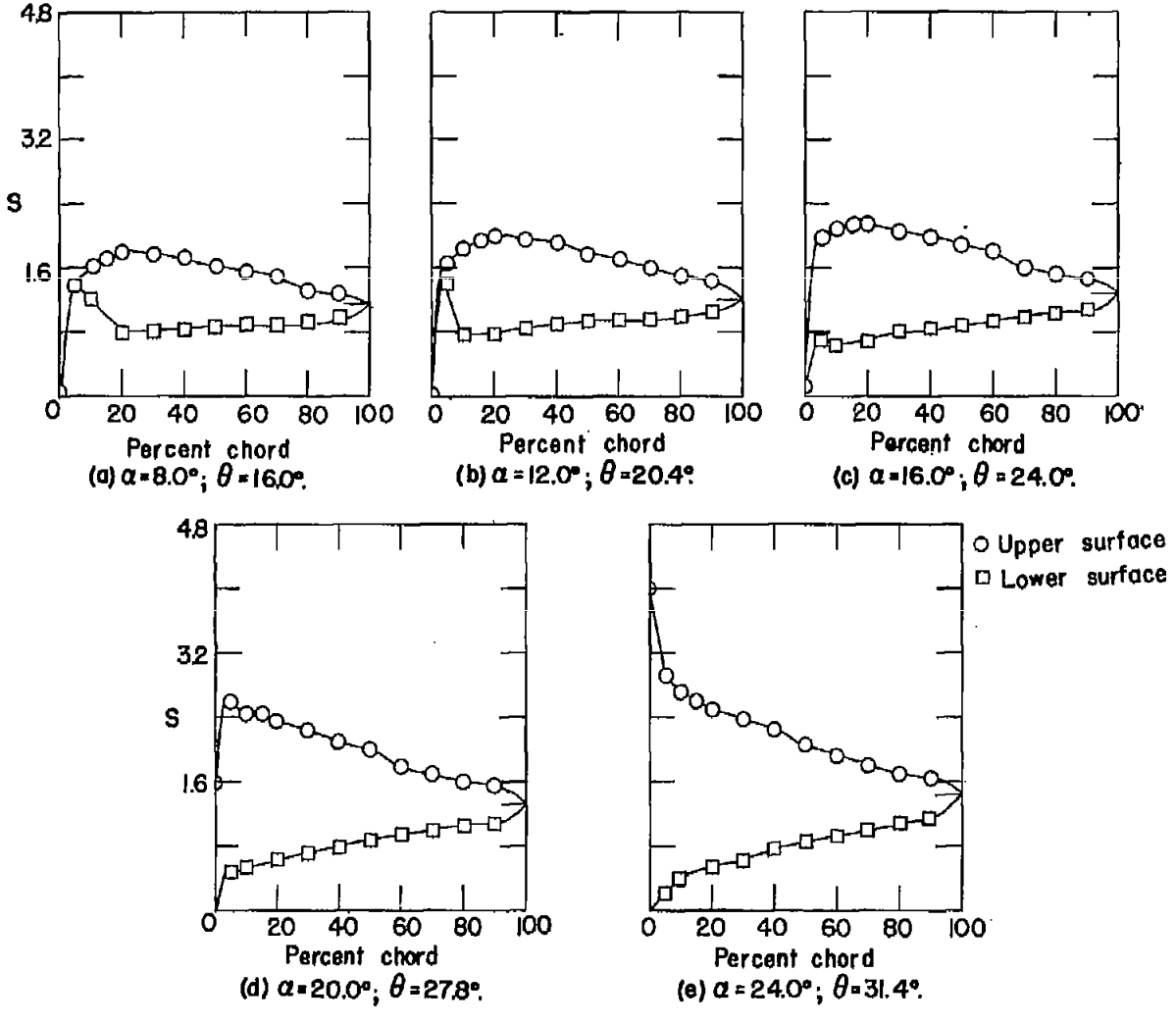

Figure 7.- Blade-surface pressure distributions and blade section characteristics for cascade combination, $\beta_1 = 0^\circ$, $\sigma = 1.0$, and NACA 63-($12A_4K_6$)06 blade section.

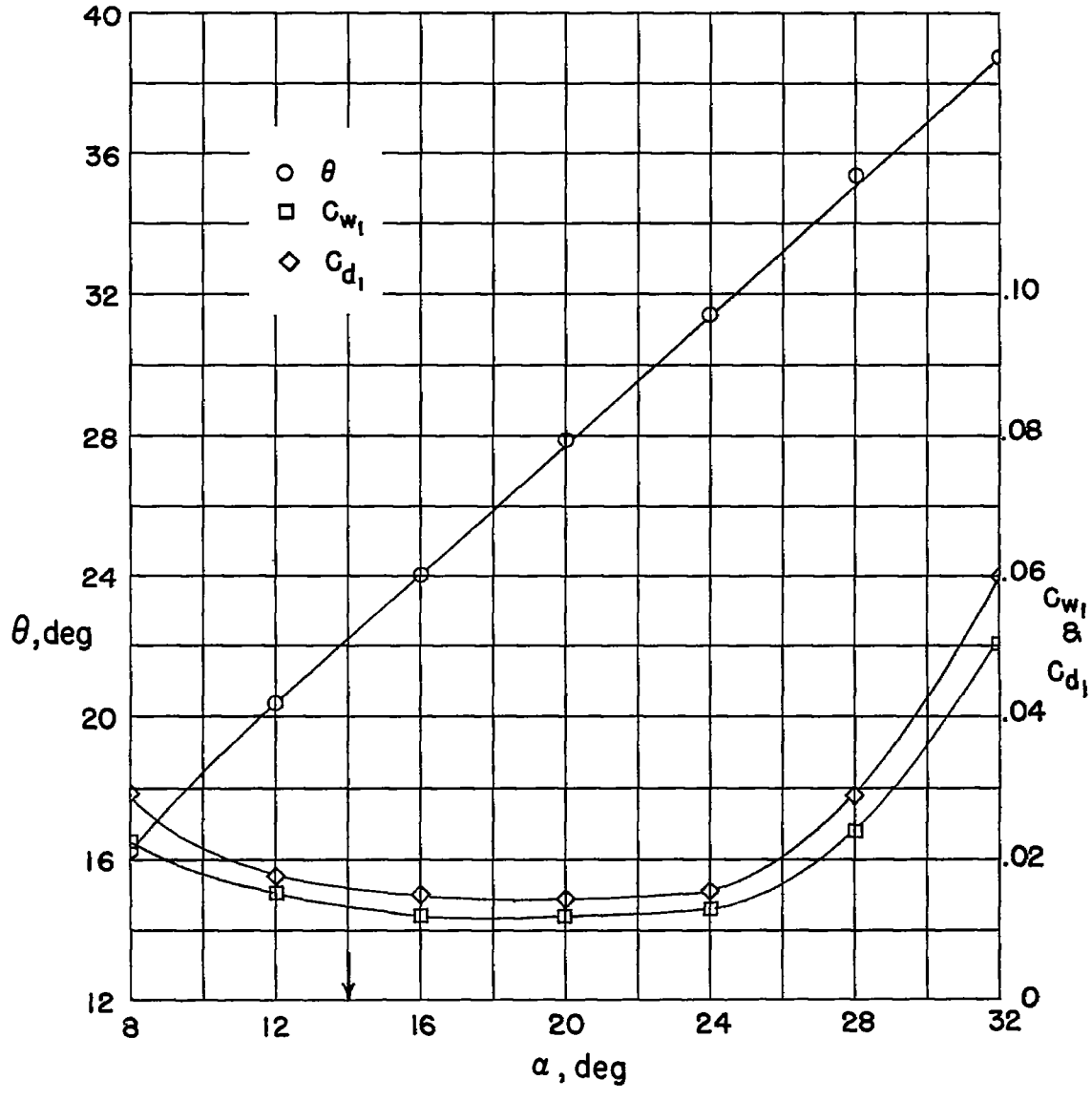

(f) Section characteristics. Arrow shows design angle of attack.

Figure 7.- Concluded.

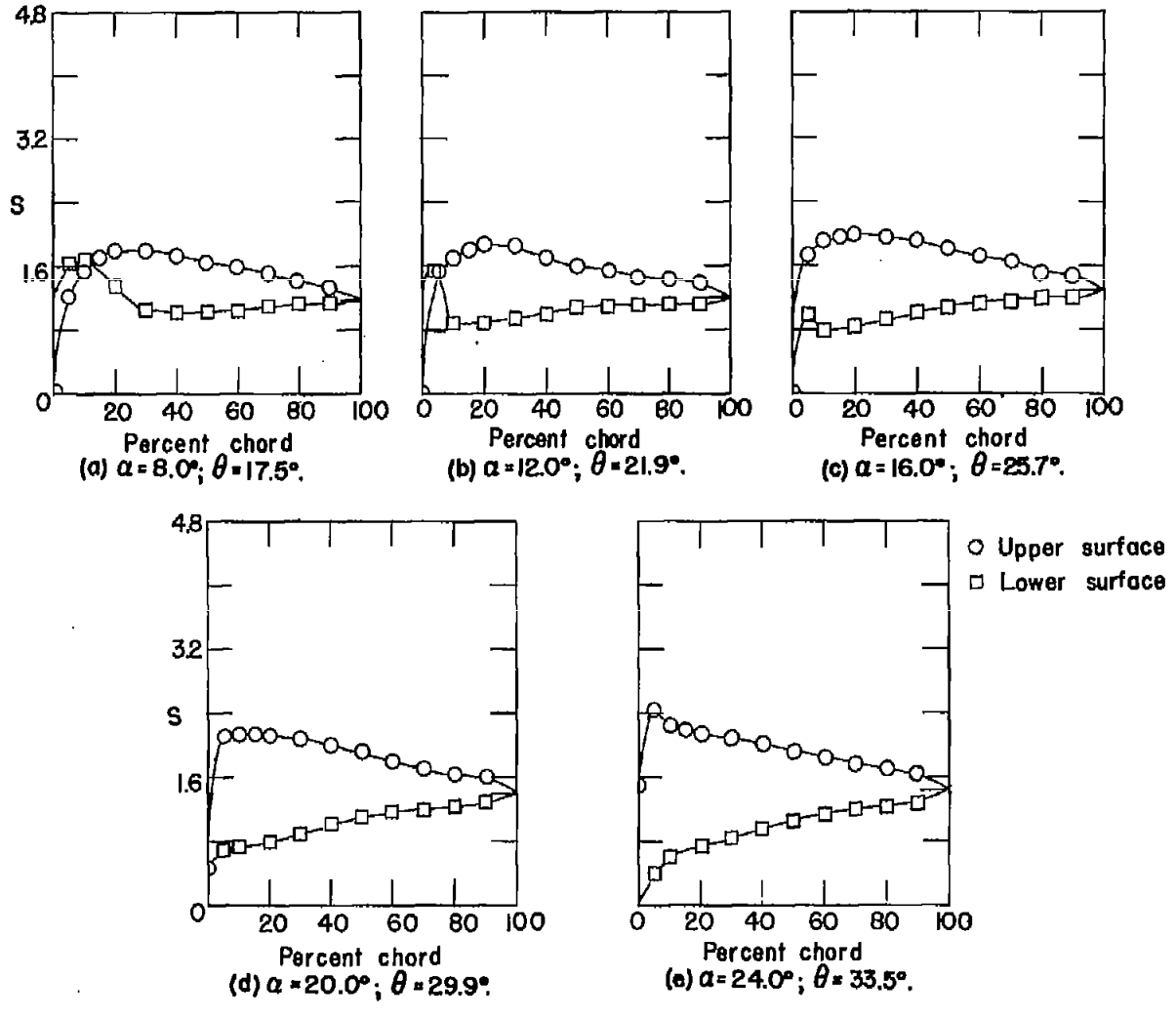

Figure 8.- Blade-surface pressure distributions and blade section characteristics for cascade combination, $\beta_1 = 0^\circ$, $\sigma = 1.5$, and NACA 63-($12A_4K_6$)06 blade section.

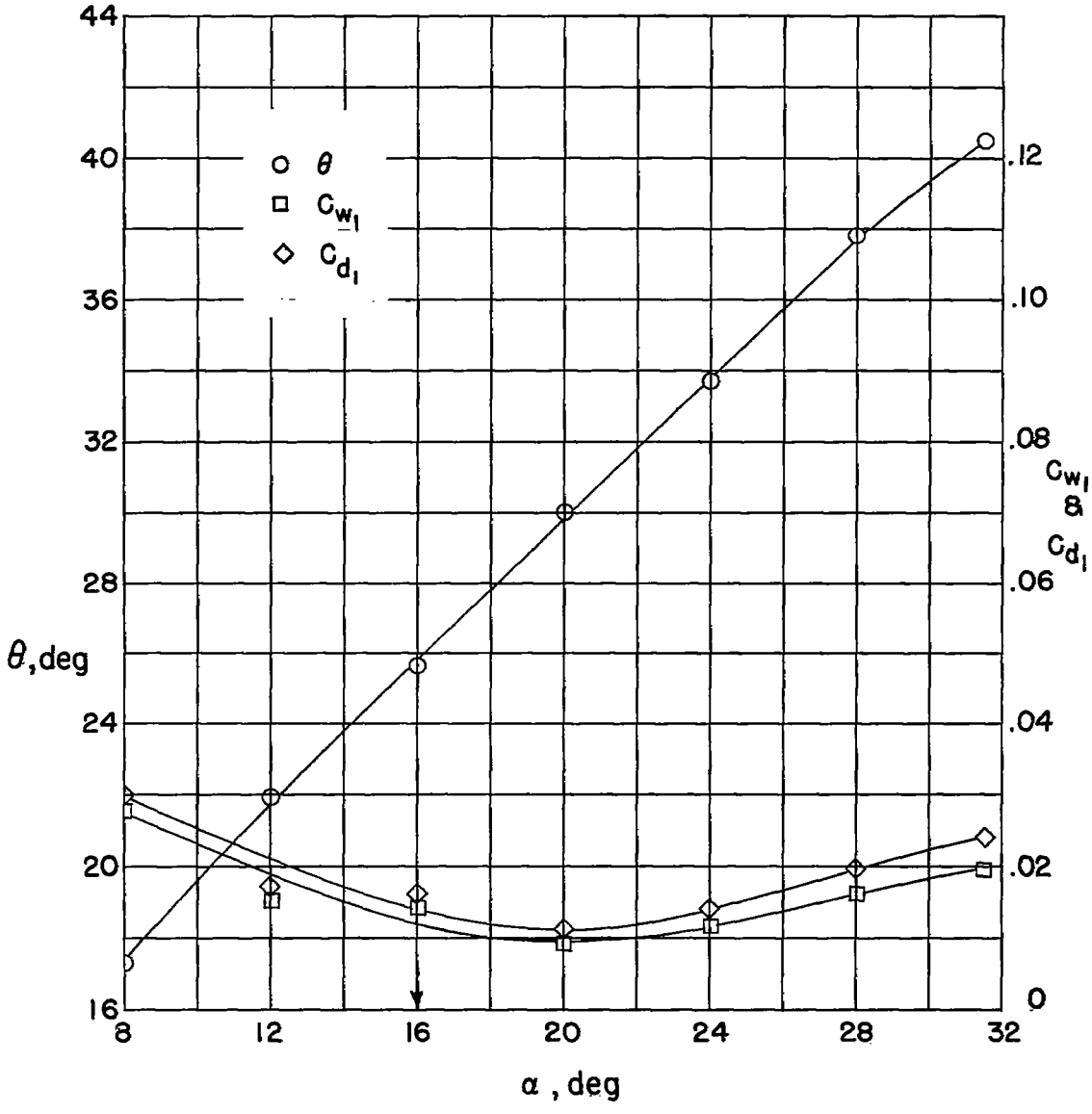

(f) Section characteristics. Arrow shows design angle of attack.

Figure 8.- Concluded.

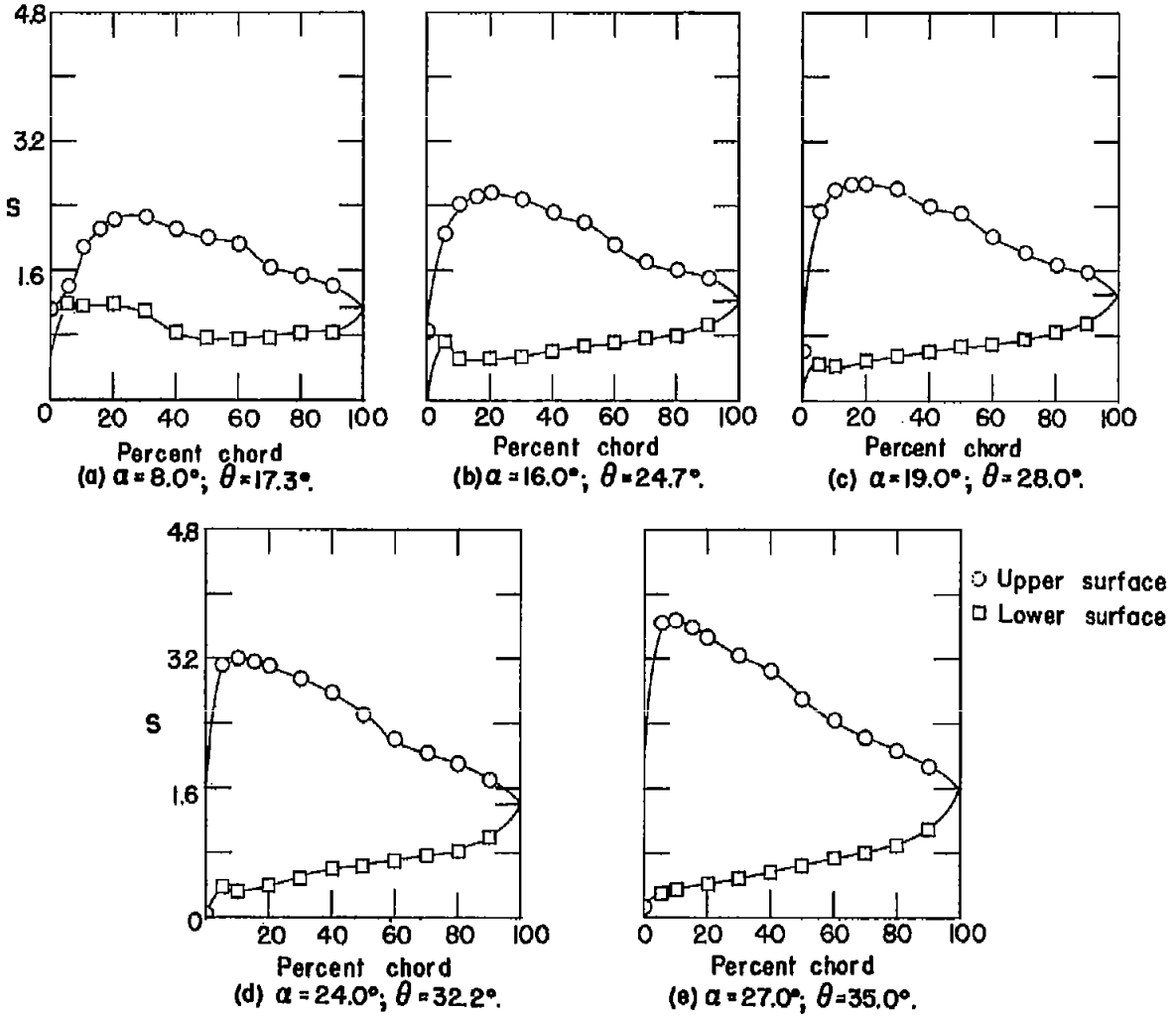

Figure 9.- Blade-surface pressure distributions and blade section characteristics for cascade combination, $\beta_1 = 0°$, $\sigma = 0.75$, and NACA 63-($18A_4K_6$)06 blade section.

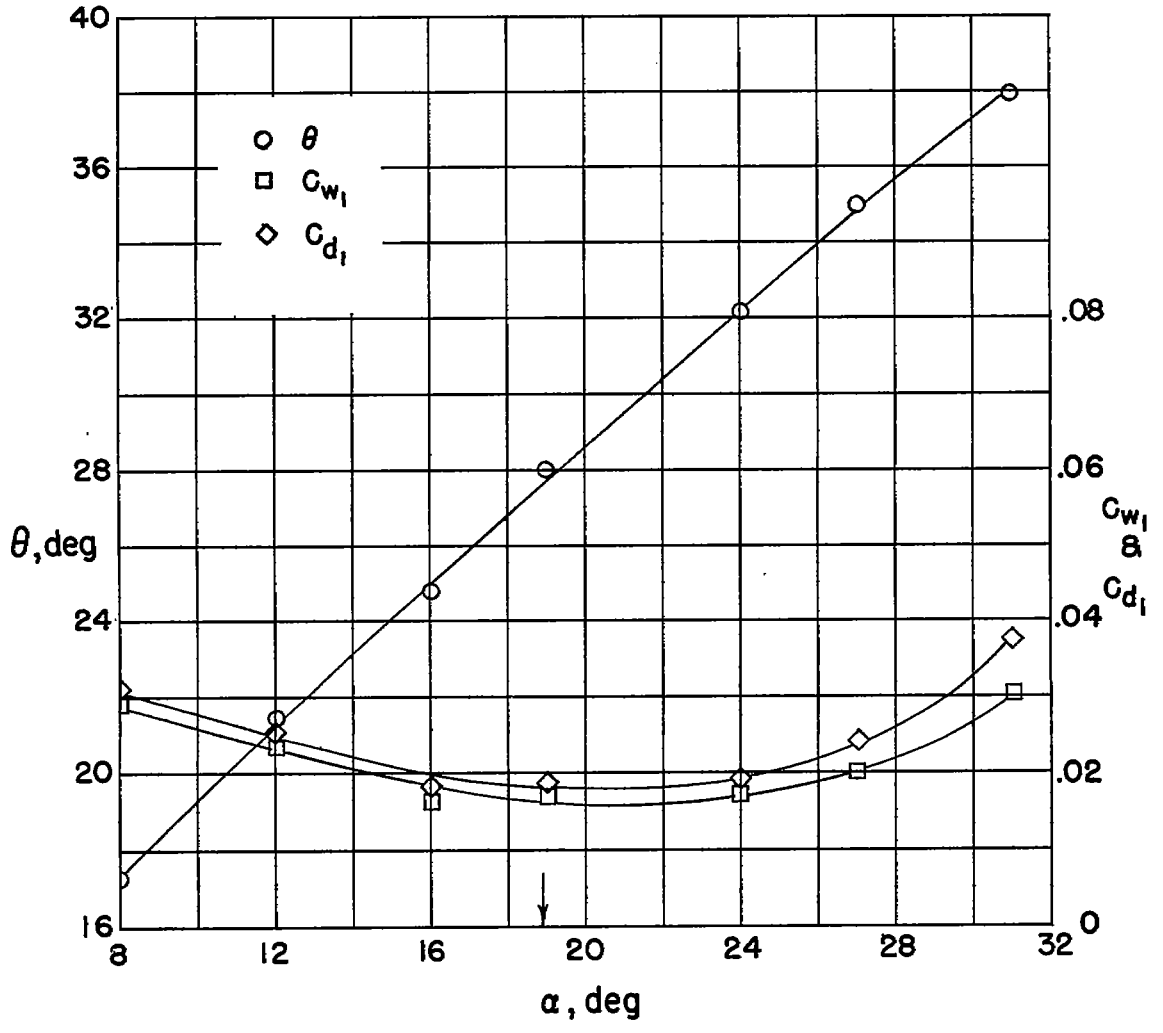

(f) Section characteristics. Arrow shows design angle of attack.

Figure 9.- Concluded.

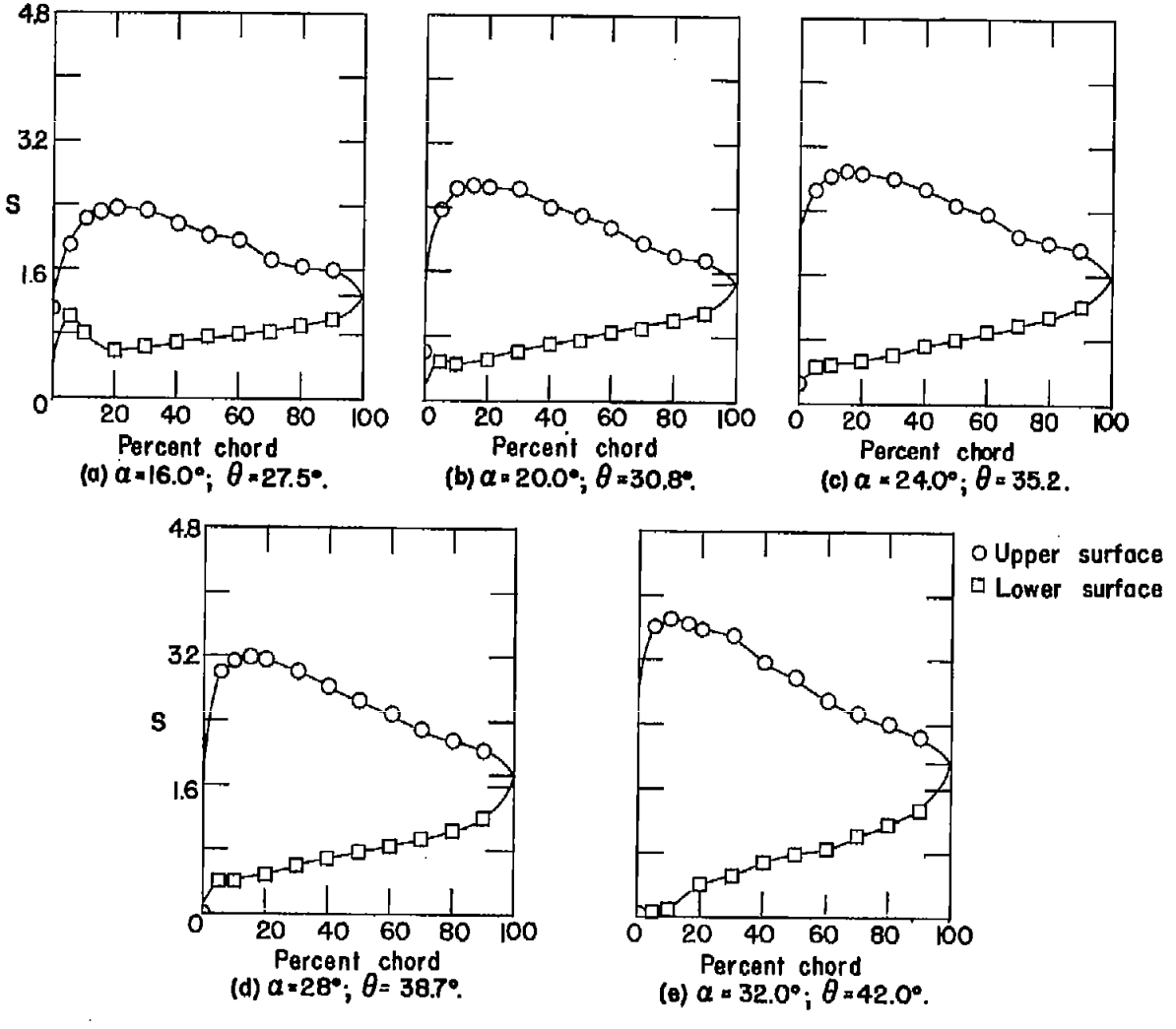

Figure 10.- Blade-surface pressure distributions and blade section characteristics for cascade combination, $\beta_1 = 0^\circ$, $\sigma = 1.0$, and NACA 63-($18A_4K_6$)06 blade section.

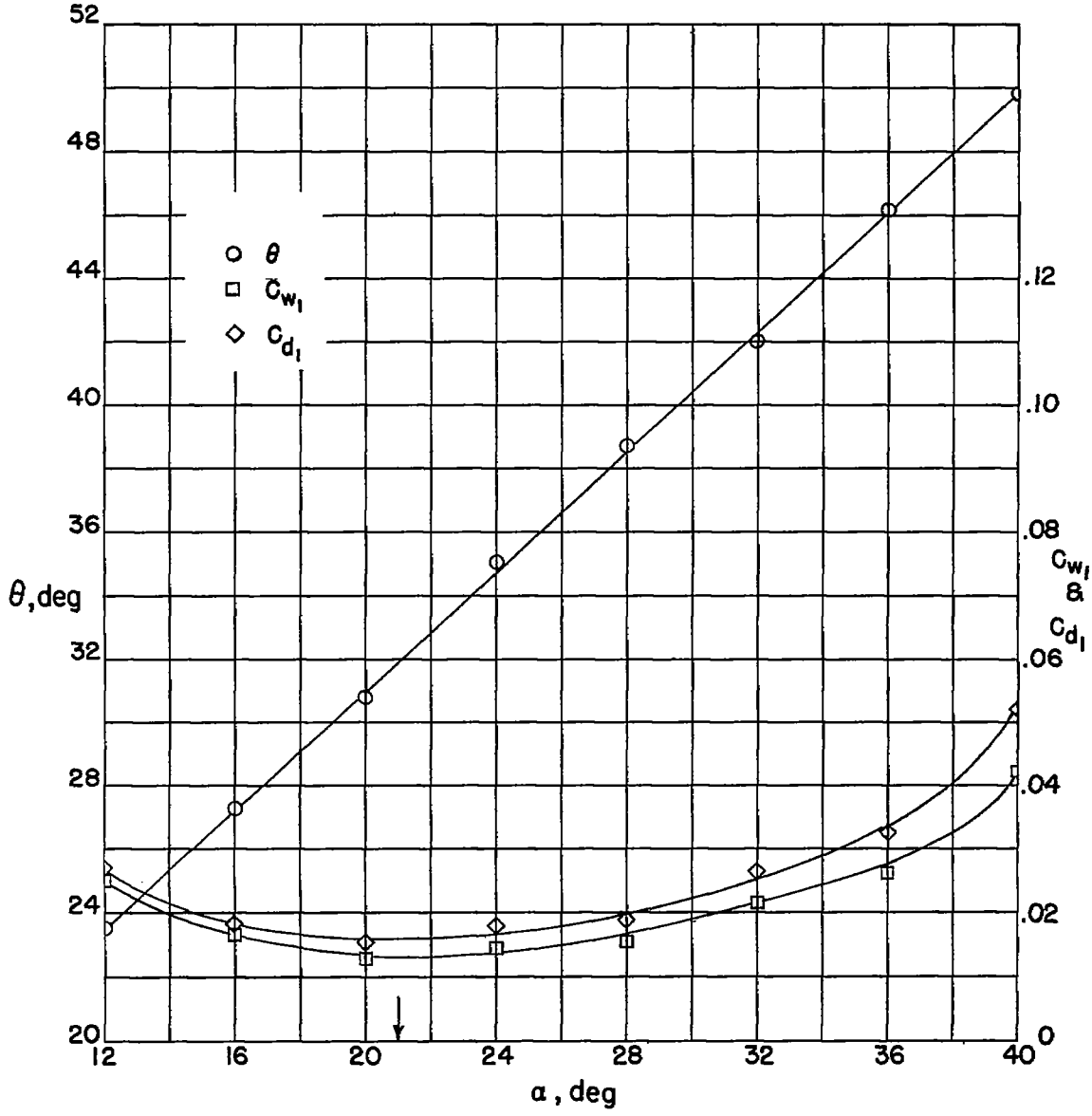

(f) Section characteristics. Arrow shows design angle of attack.

Figure 10.- Concluded.

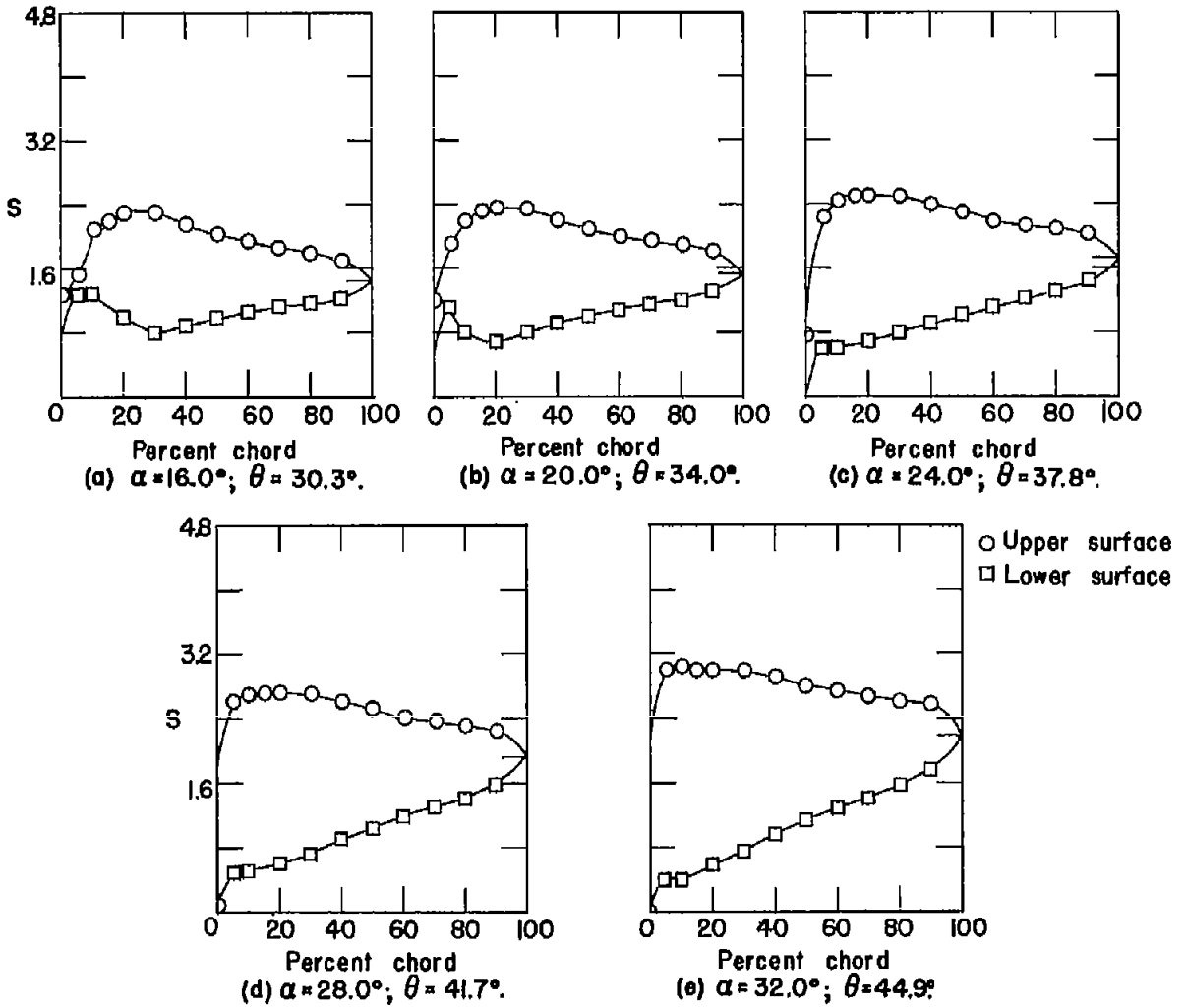

Figure 11.- Blade-surface pressure distributions and blade section characteristics for cascade combination, $\beta_1 = 0^\circ$, $\sigma = 1.5$, and NACA 63-($18A_4K_6$)06 blade section.

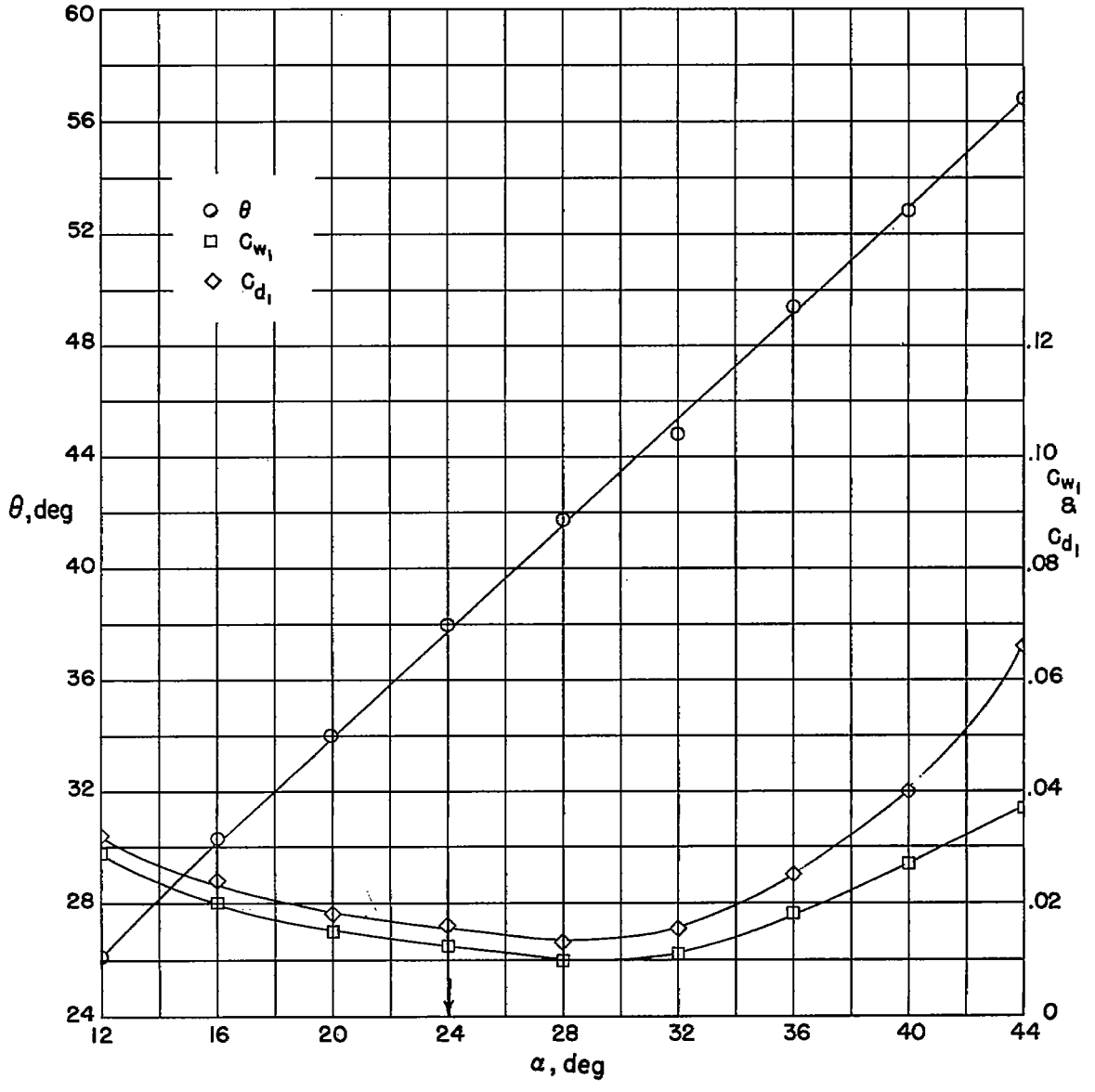

(f) Section characteristics. Arrow shows design angle of attack.

Figure 11.- Concluded.

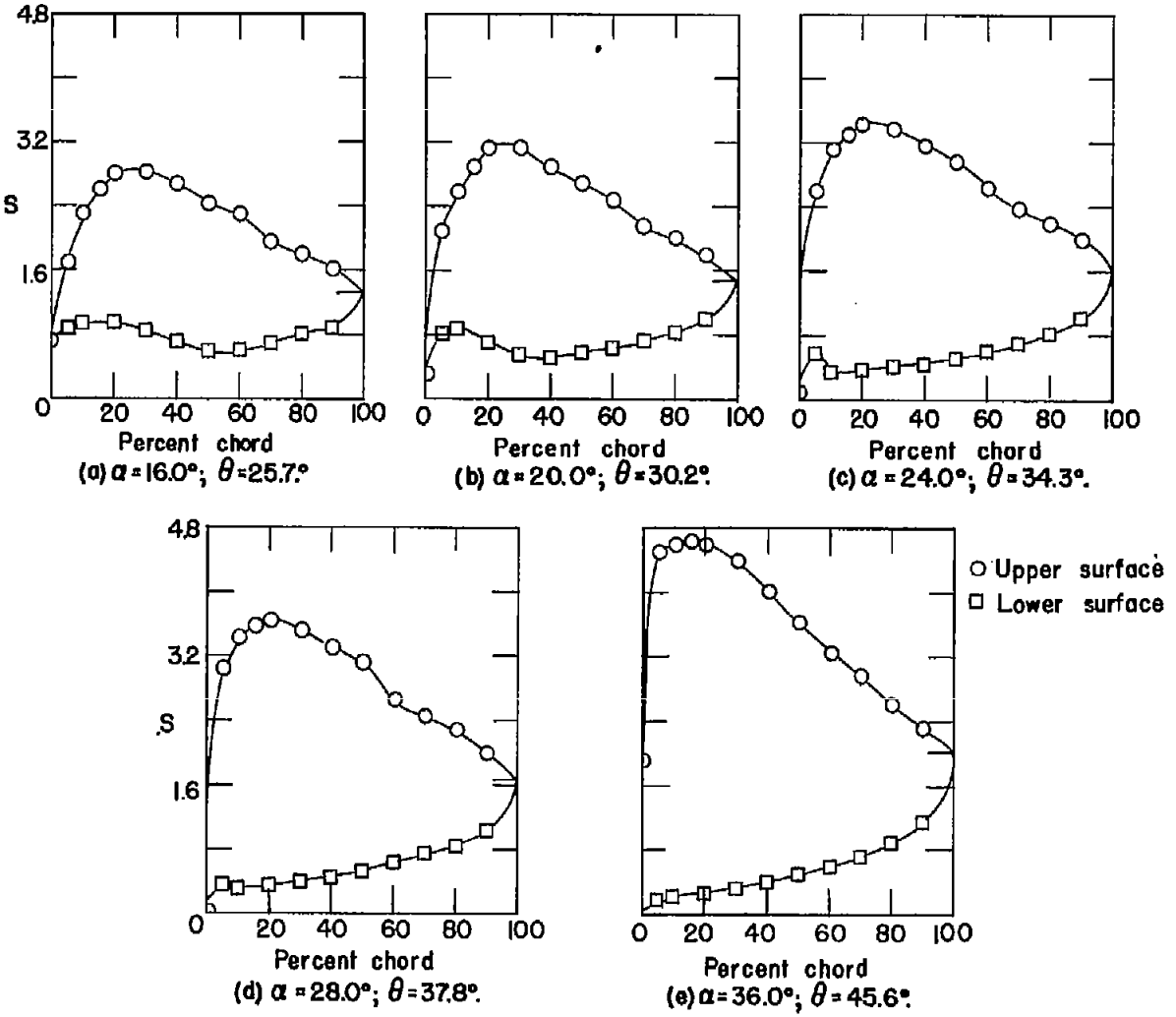

Figure 12.- Blade-surface pressure distributions and blade section characteristics for cascade combination, $\beta_1 = 0^\circ$, $\sigma = 0.75$, and NACA 63-($24A_4K_6$)06 blade section.

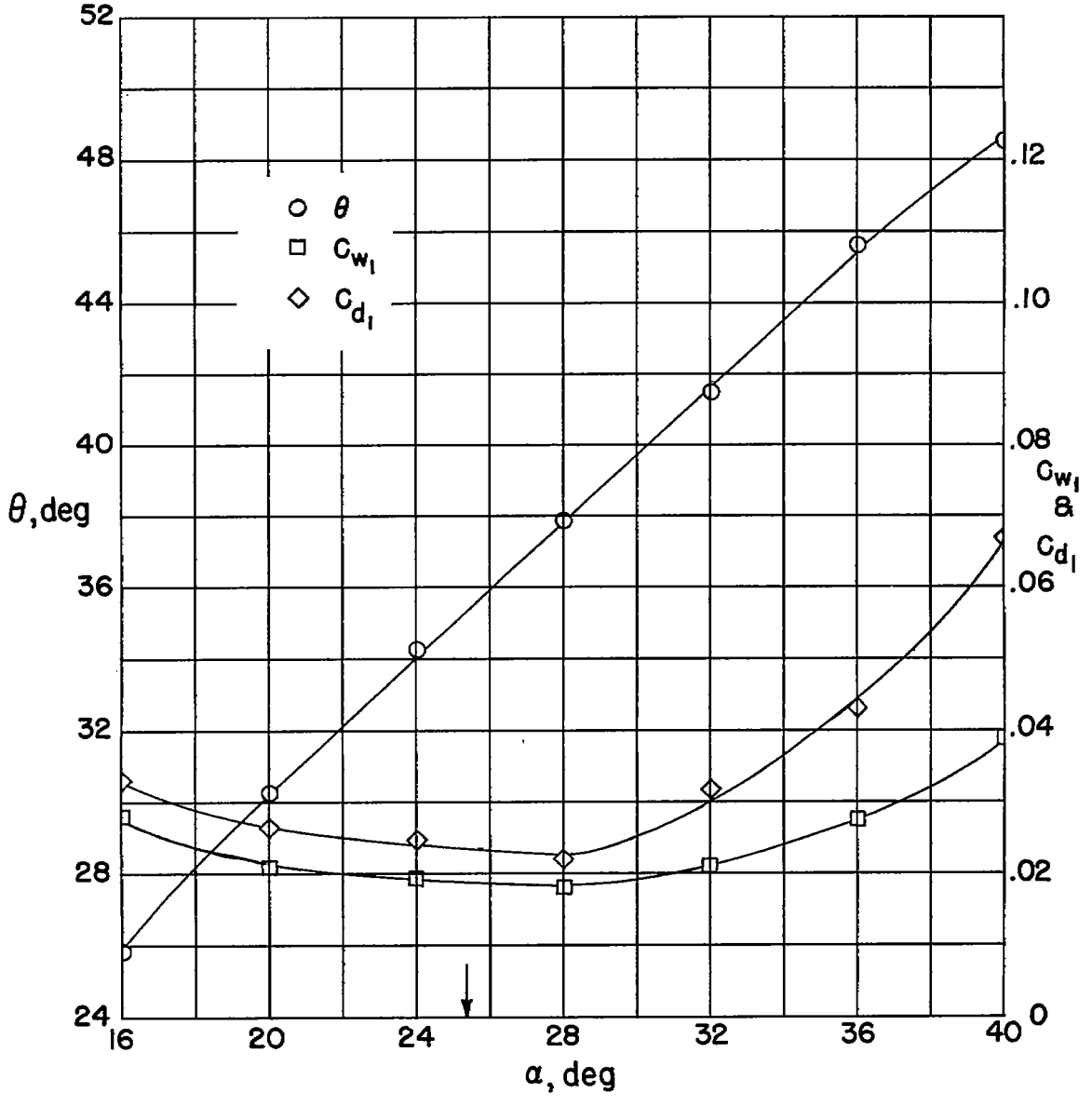

(f) Section characteristics. Arrow shows design angle of attack.

Figure 12.- Concluded.

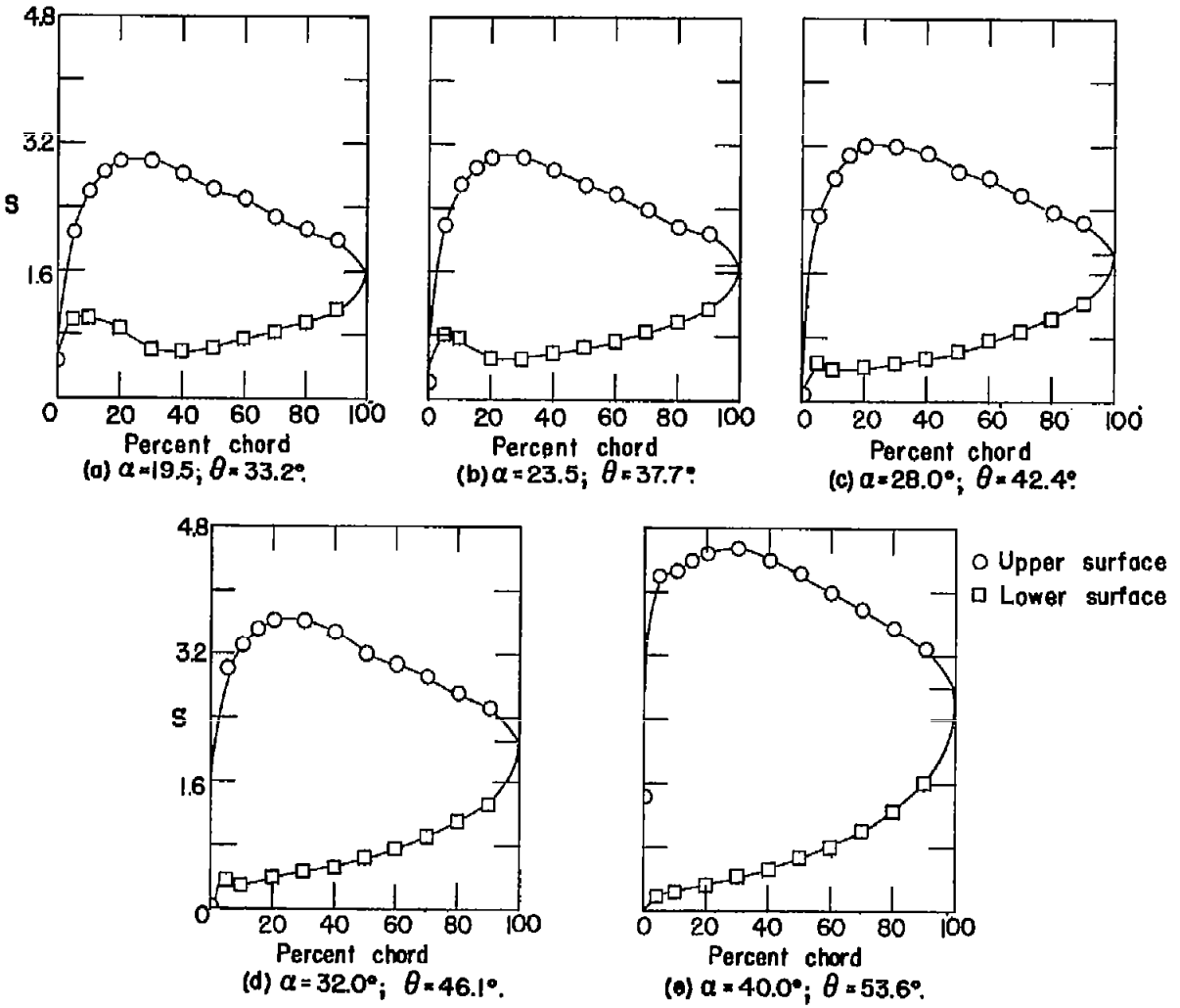

Figure 13.- Blade-surface pressure distributions and blade section characteristics for cascade combination, $\beta_1 = 0^\circ$, $\sigma = 1.0$, and NACA 63-(24A4K6)06 blade section.

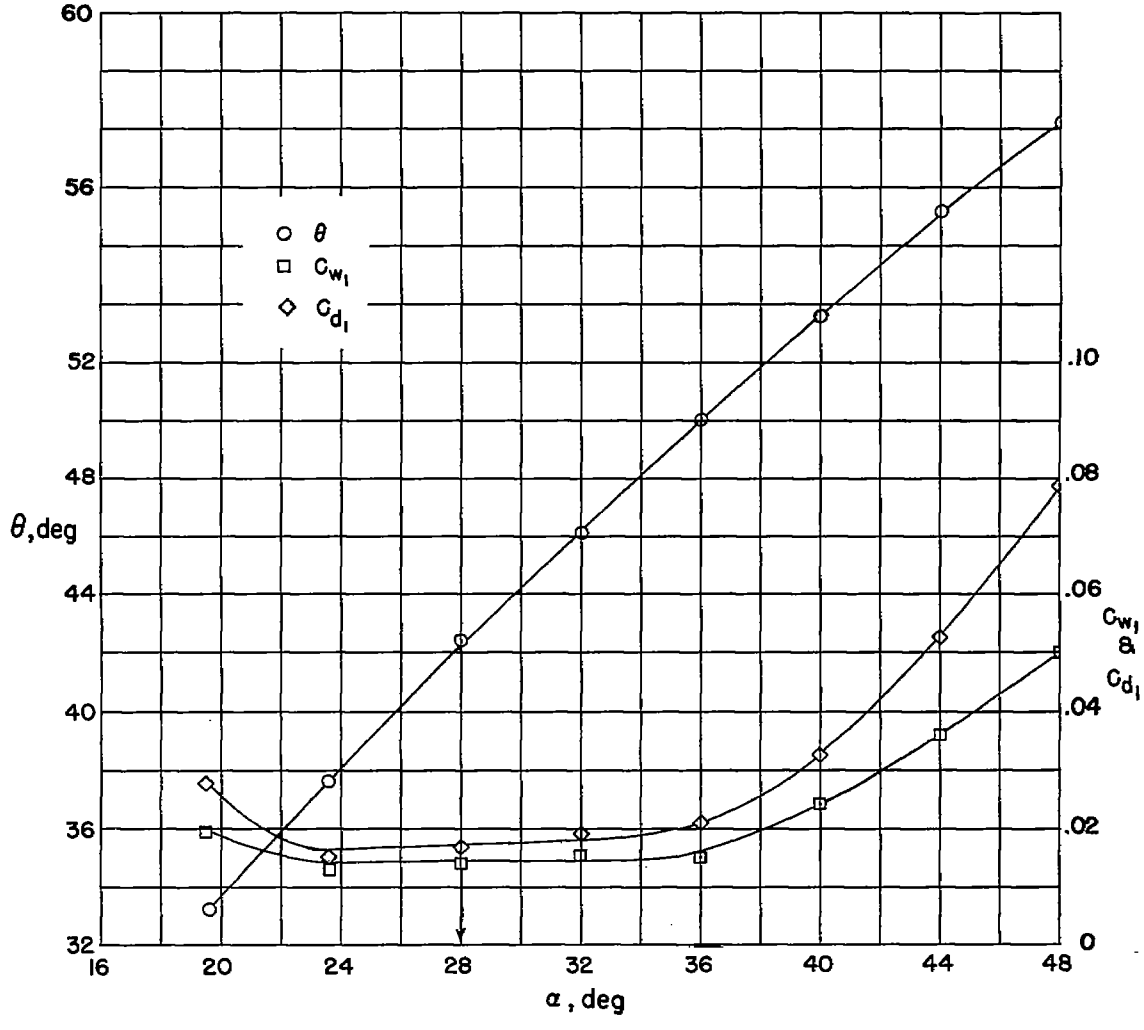

(f) Section characteristics. Arrow shows design angle of attack.

Figure 13.- Concluded.

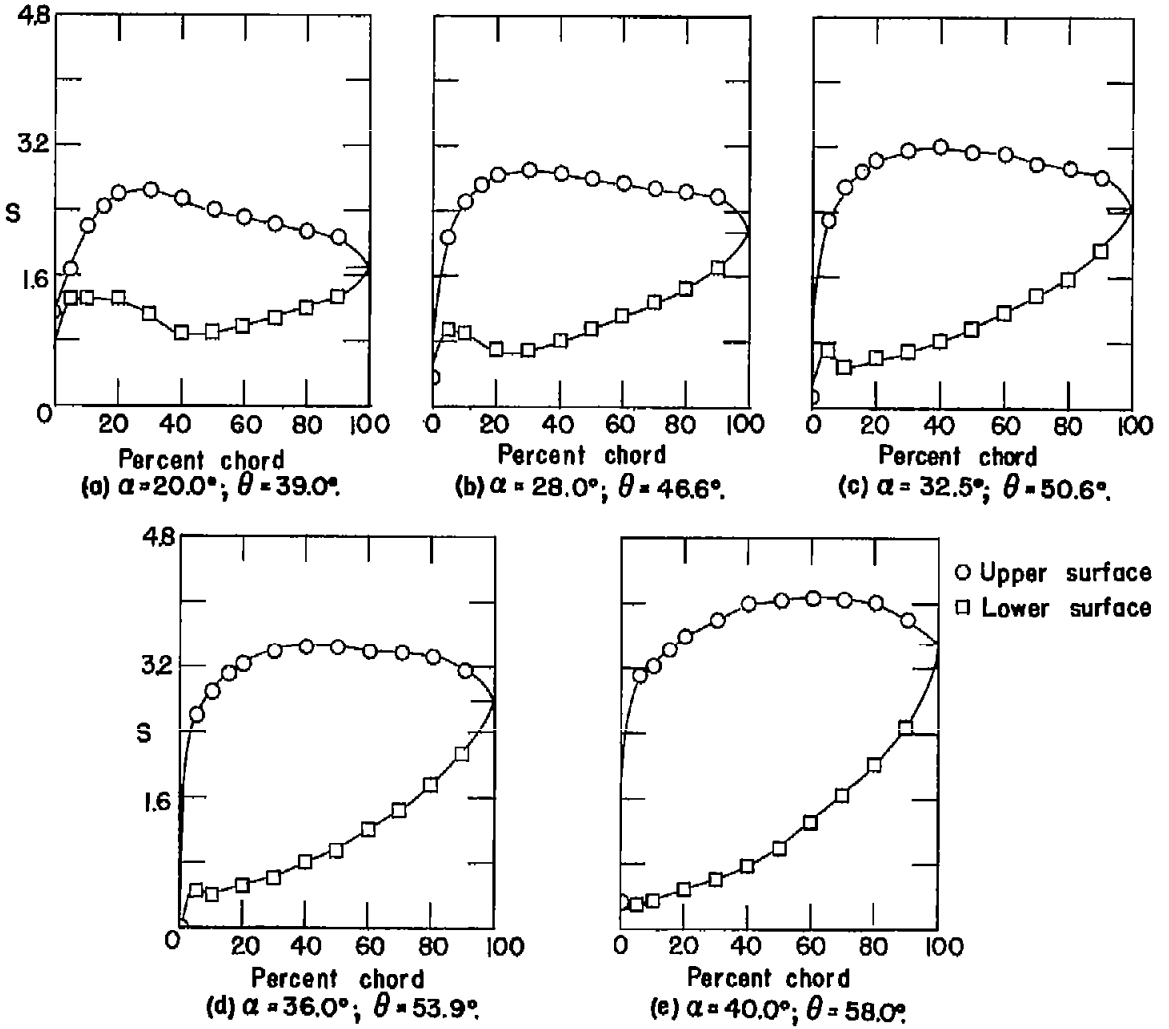

Figure 14.- Blade-surface pressure distributions and blade section characteristics for cascade combination, $\beta_1 = 0^\circ$, $\sigma = 1.5$, and NACA 63-($24A_4K_6$)06 blade section.

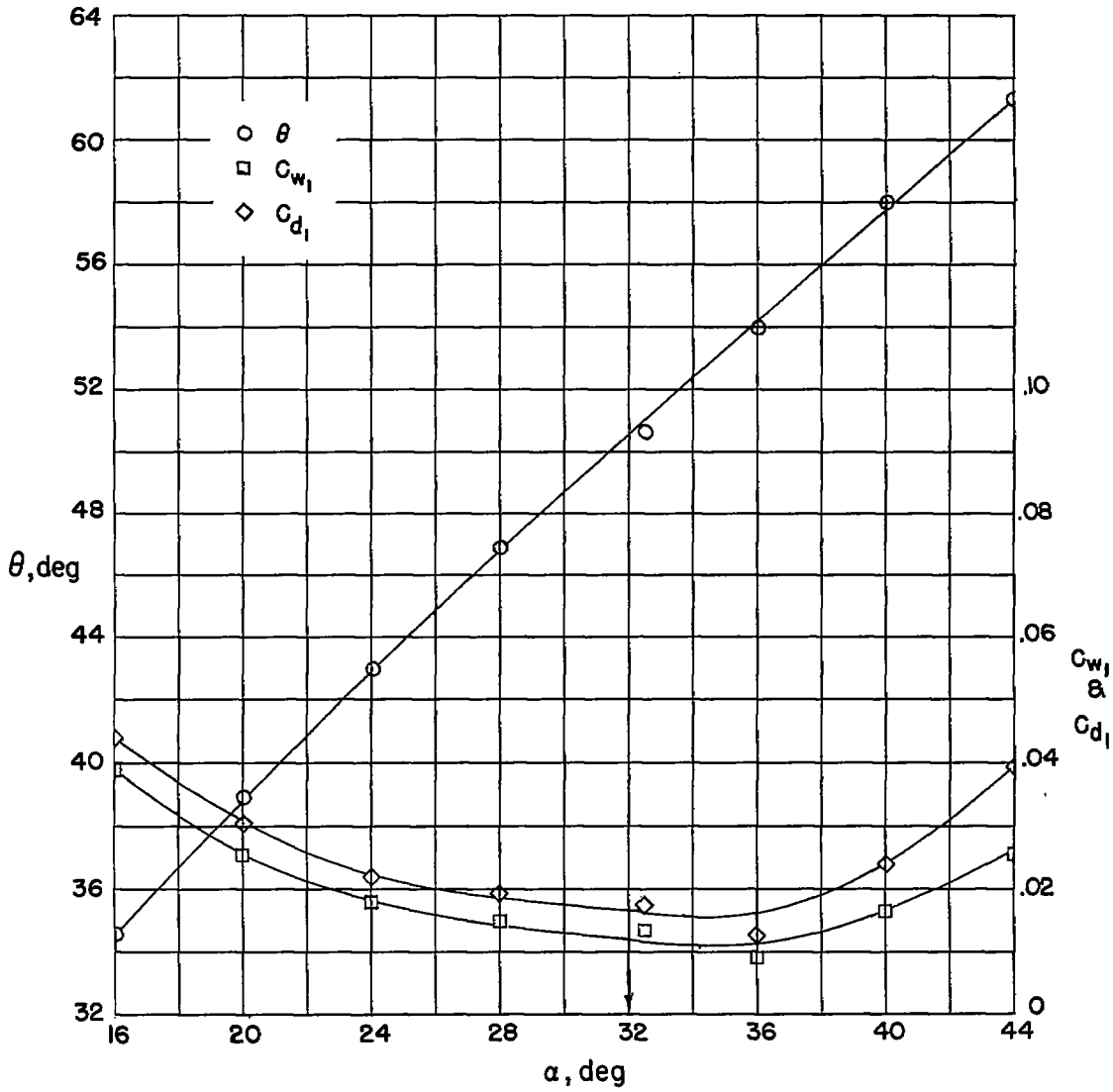

(f) Section characteristics. Arrow shows design angle of attack.

Figure 14.- Concluded.

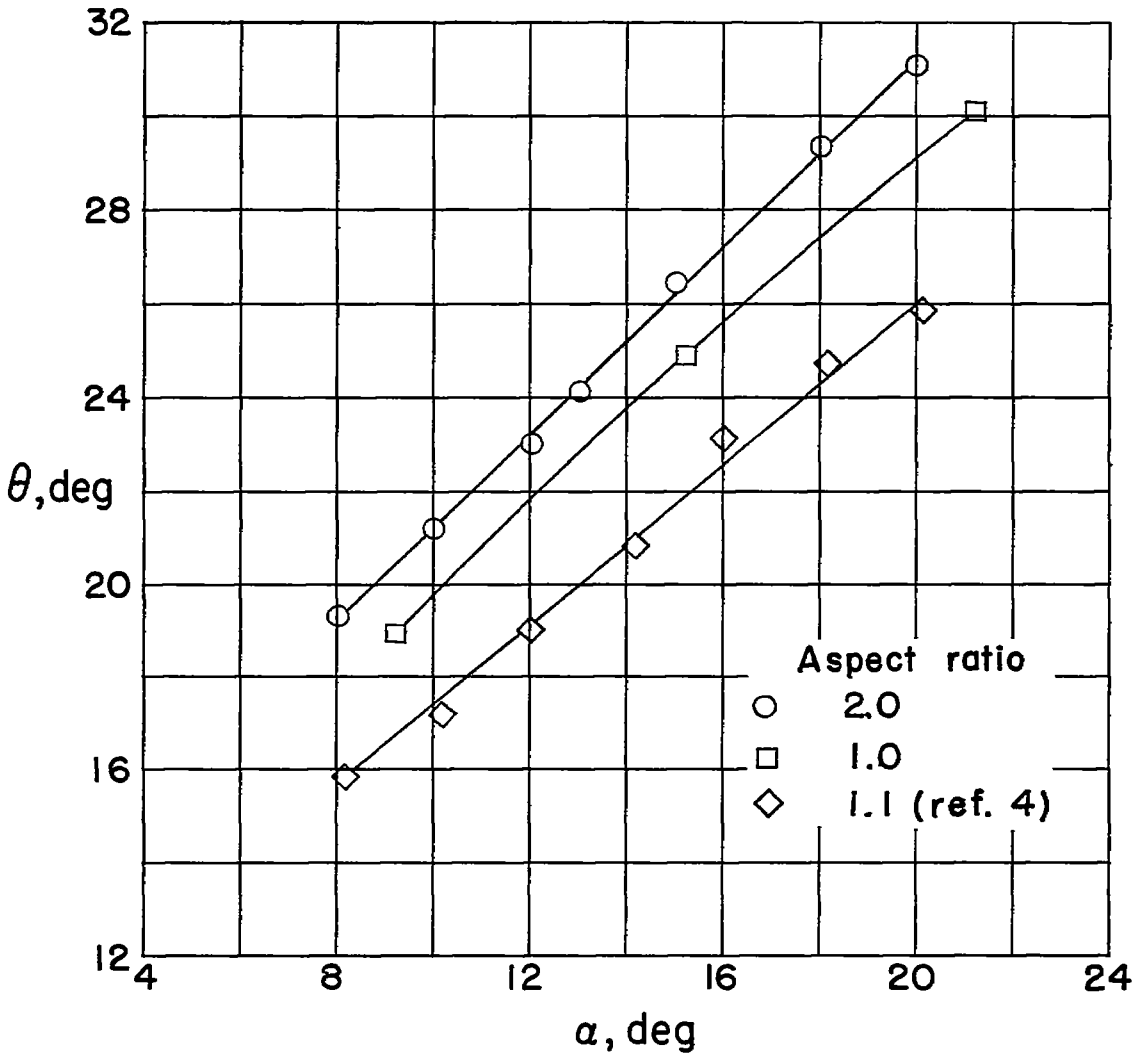

(a) $\sigma = 1.0$.

Figure 15.- Cascade turning angles for NACA 65-$(12A_{10})10$ blade section at $\beta_1 = 0^\circ$.

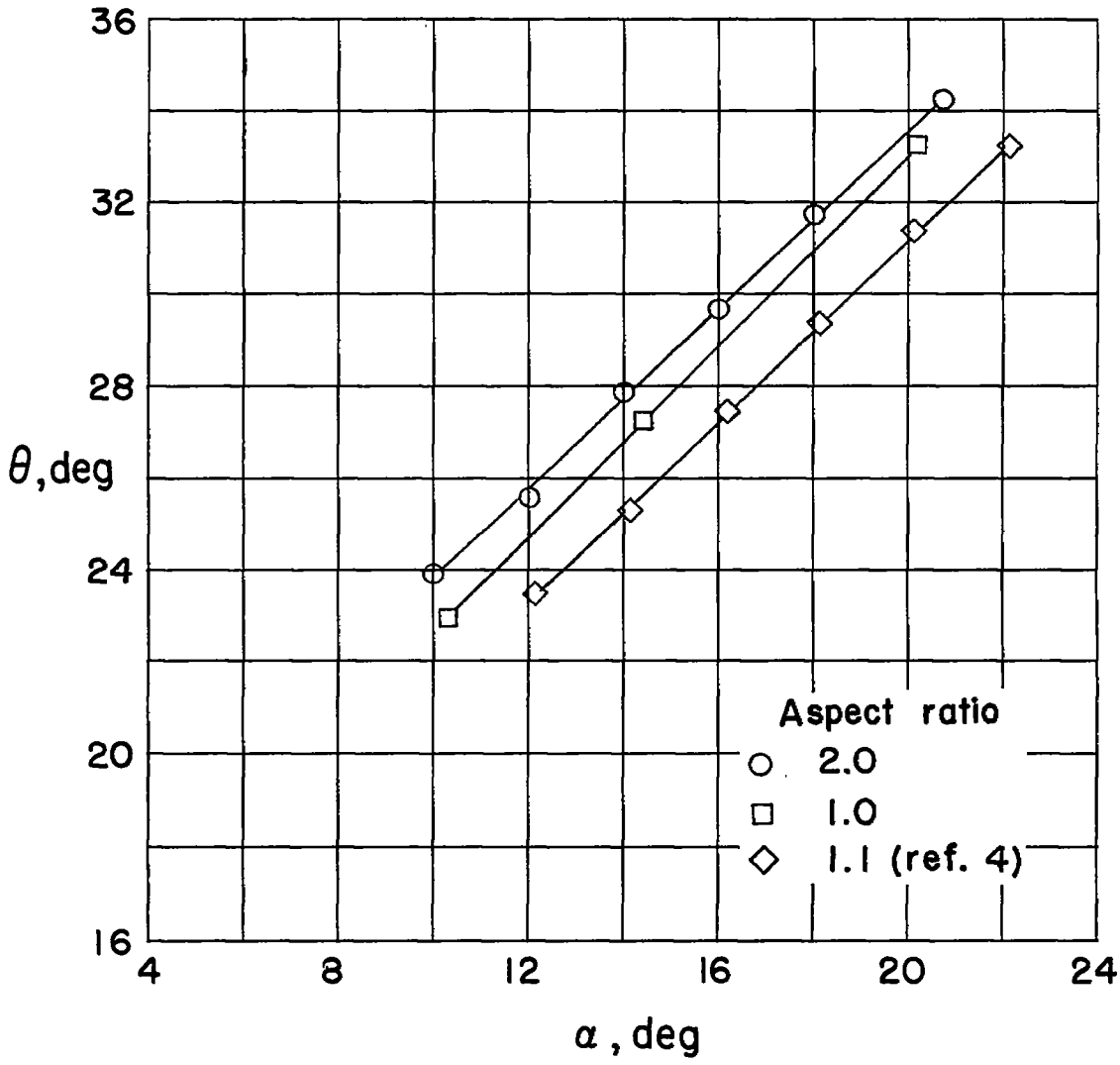

(b) $\sigma = 1.5$.

Figure 15.- Concluded.

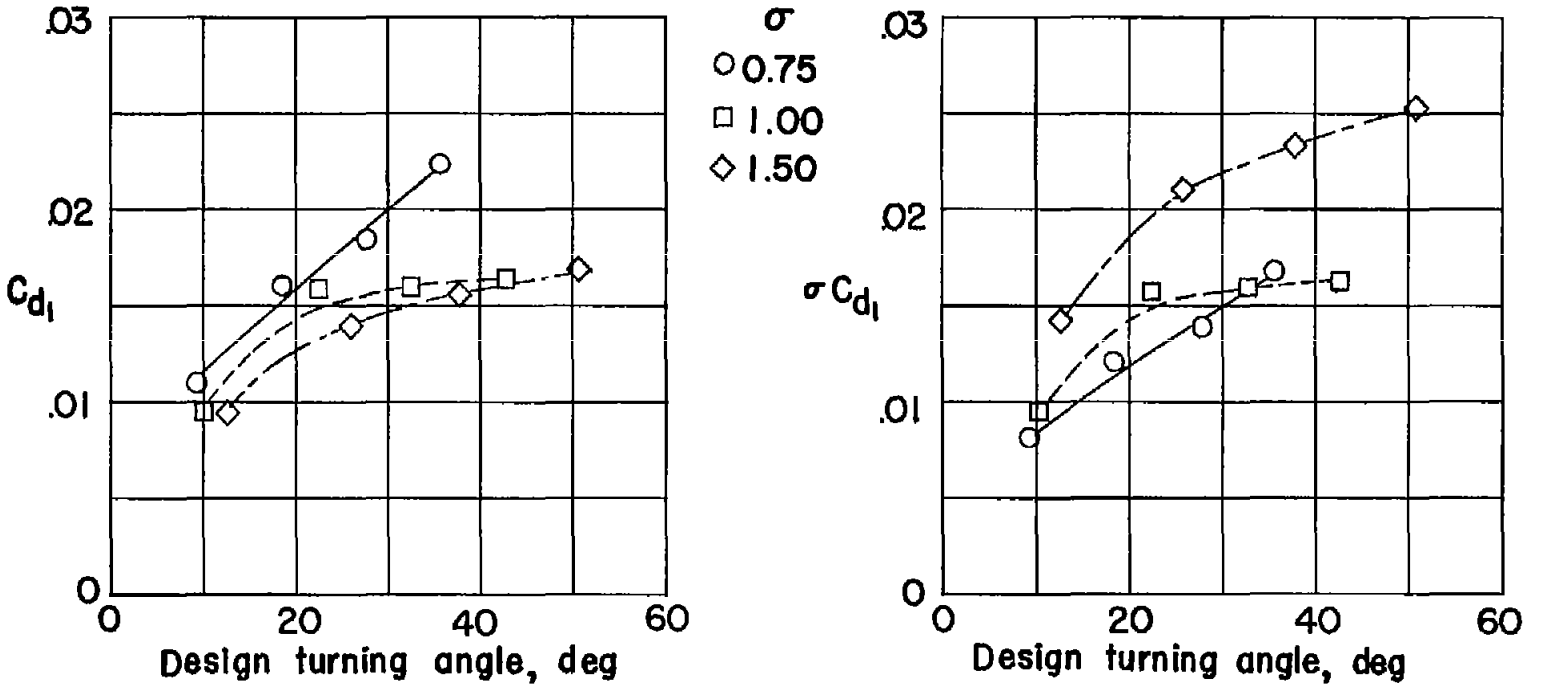

(a) Drag coefficient.

(b) Product of solidity and drag coefficient.

Figure 16.- Low-speed drag coefficient for the NACA 63-$\left(C_{l_o} A_4 K_6\right)$06 guide-vane blade series at design angle of attack.

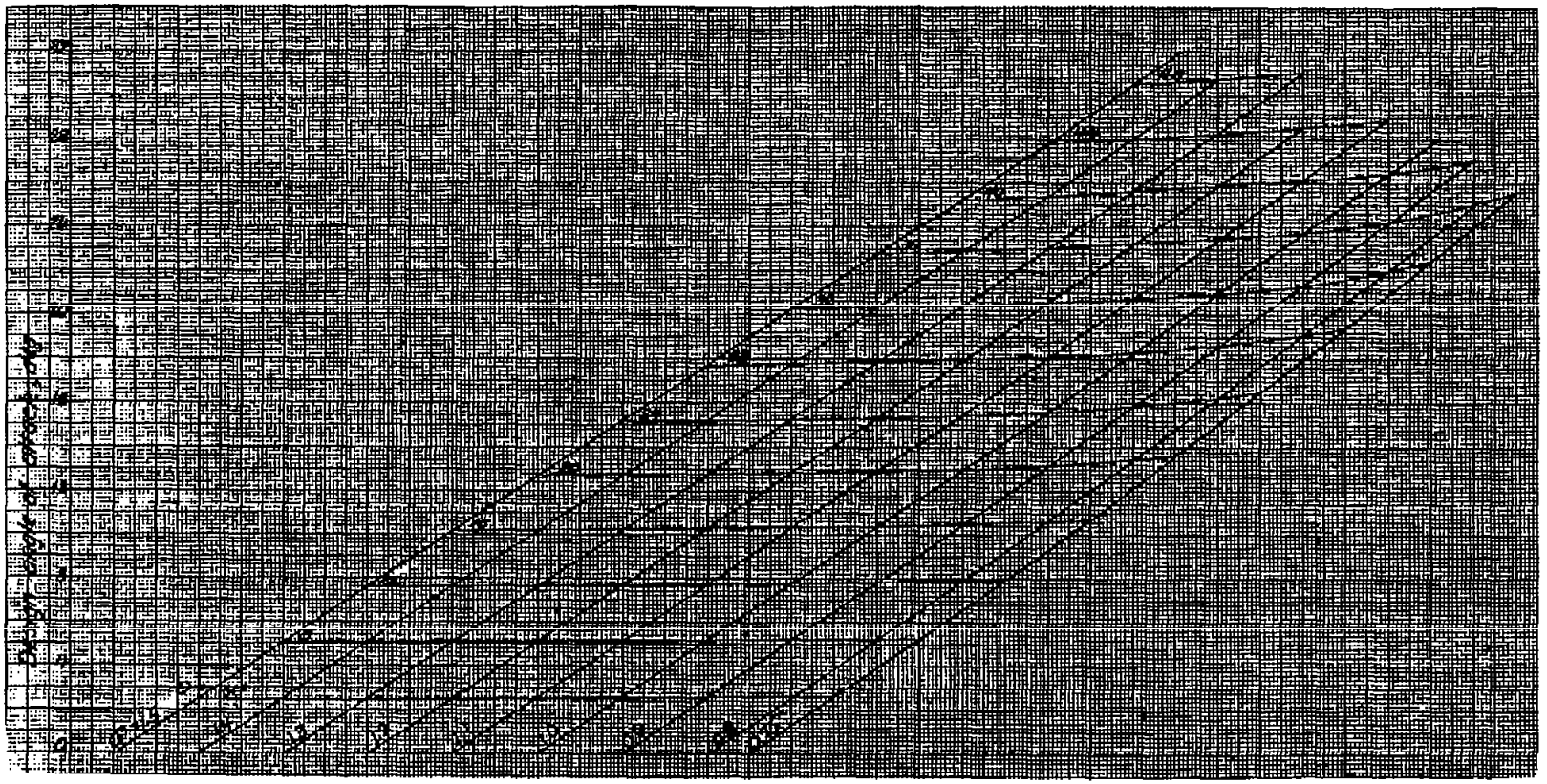

Figure 17.- Design angle of attack for the NACA 63-$(C_{l_o}A_4K_6)$06 guide-vane blade series.

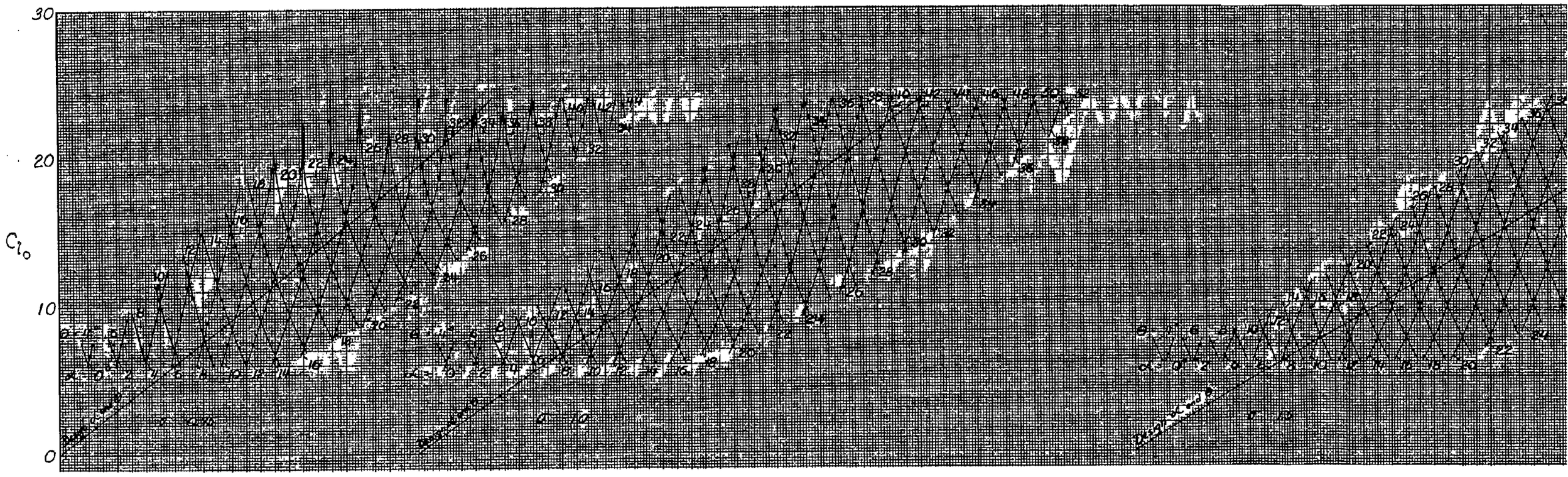

Figure 18.- θ,α,σ carpet plot for NACA 63-$\left(C_{l_0}A_4K_6\right)$06 guide-vane series.

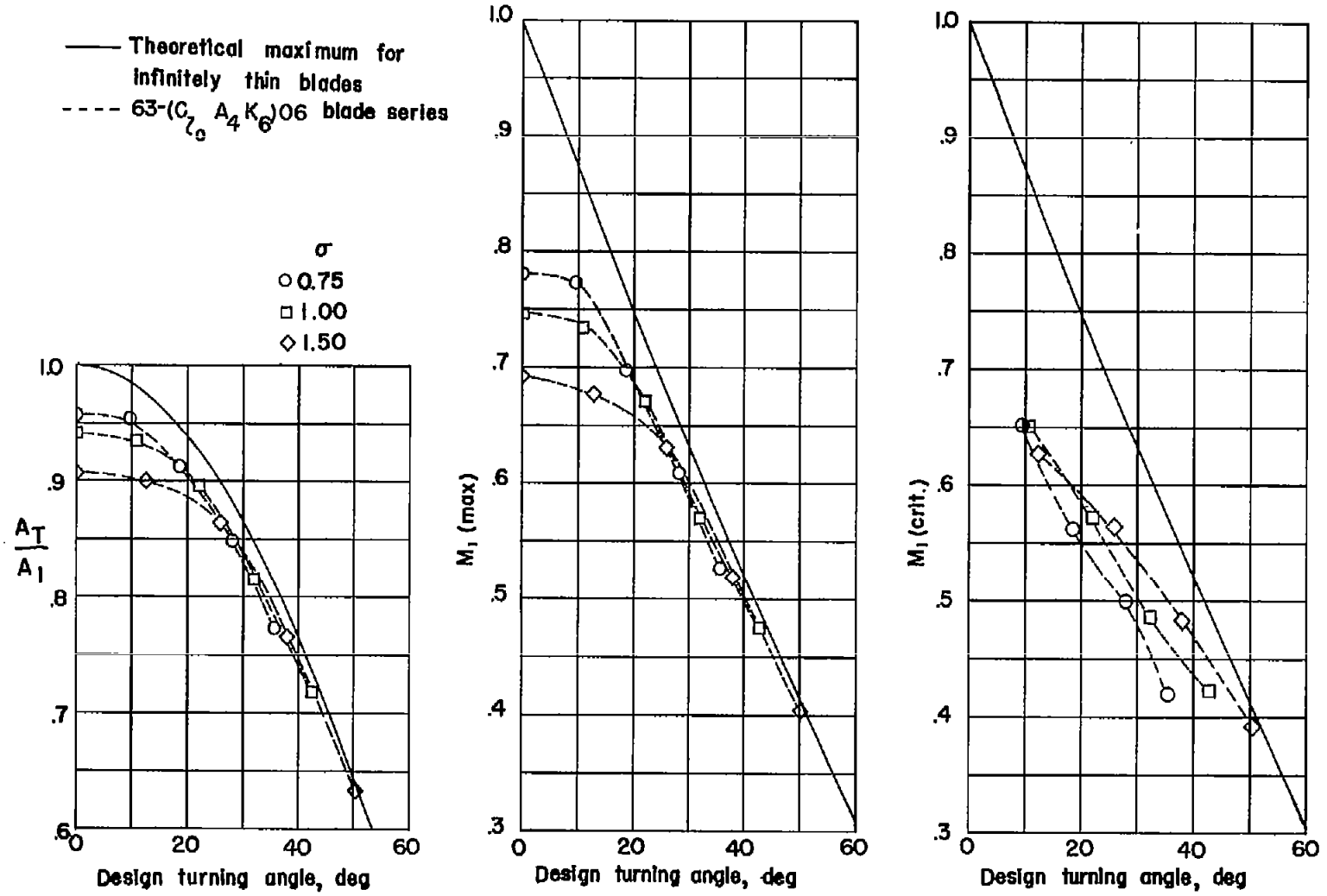

(a) Blade passage throat area. (b) Maximum entering Mach number. (c) Critical Mach number.

Figure 19.- Characteristics of NACA 63-$\left(C_{l_o} A_4 K_6\right)$06 guide-vane blade series.

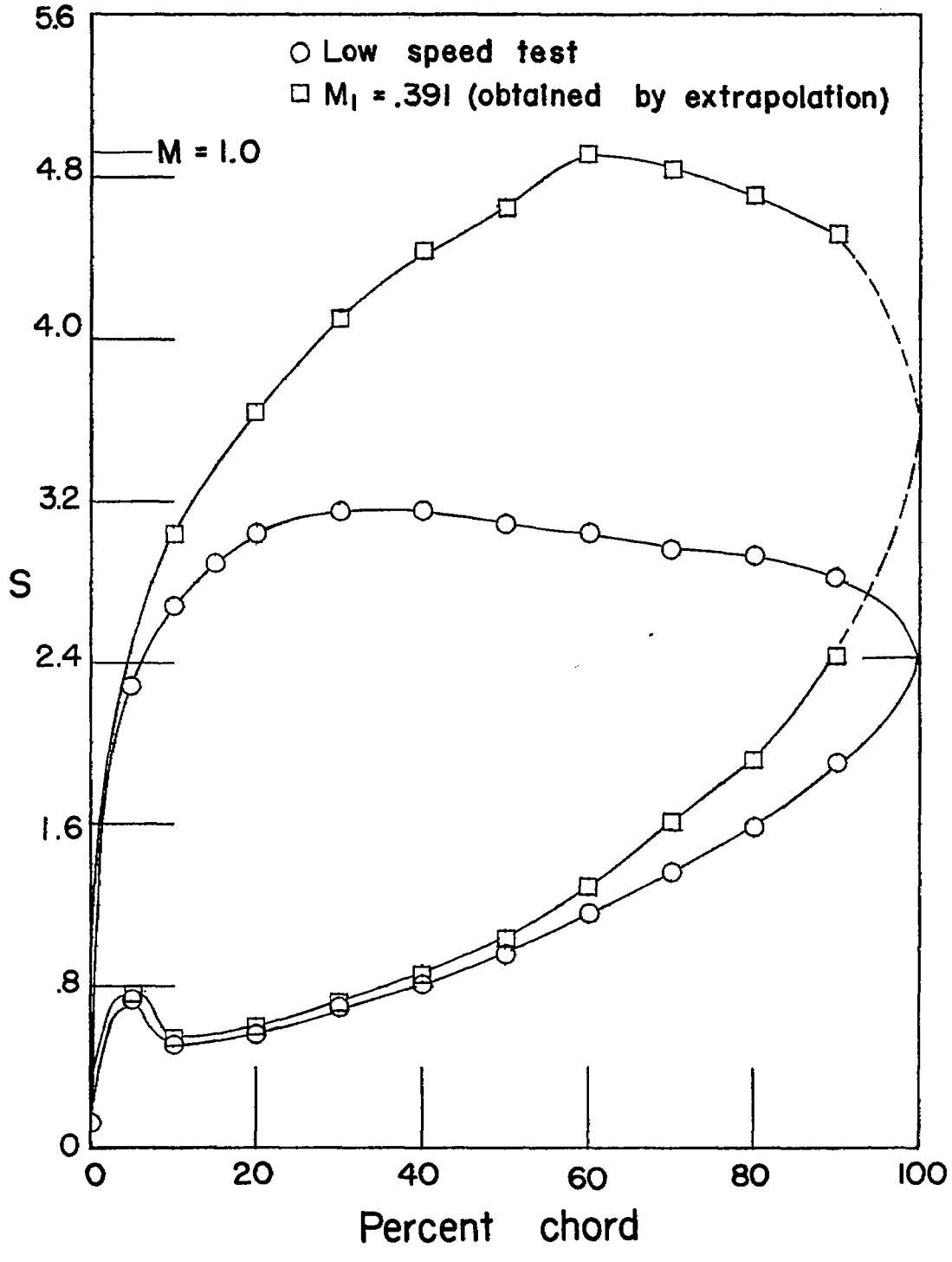

Figure 20.- Low-speed and extrapolated pressure distributions for NACA 63-($24A_4K_6$)06 blade section. $\alpha = 32.5^\circ$; $\sigma = 1.5$; $\theta = 50.6^\circ$.